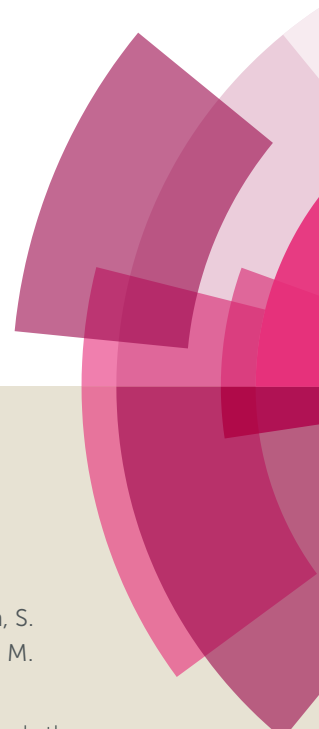


# NJC

Accepted Manuscript



This article can be cited before page numbers have been issued, to do this please use: M. A. A. Subhan, S. S. Jhuma, P. Chandra Saha, M. M. Alam, A. M. Asiri, M. Al-Mamun, S. A. Attia, T. H. Emon, A. K. Azad and M. M. Rahman, *New J. Chem.*, 2019, DOI: 10.1039/C9NJ01760G.



This is an Accepted Manuscript, which has been through the Royal Society of Chemistry peer review process and has been accepted for publication.

Accepted Manuscripts are published online shortly after acceptance, before technical editing, formatting and proof reading. Using this free service, authors can make their results available to the community, in citable form, before we publish the edited article. We will replace this Accepted Manuscript with the edited and formatted Advance Article as soon as it is available.

You can find more information about Accepted Manuscripts in the [author guidelines](#).

Please note that technical editing may introduce minor changes to the text and/or graphics, which may alter content. The journal's standard [Terms & Conditions](#) and the ethical guidelines, outlined in our [author and reviewer resource centre](#), still apply. In no event shall the Royal Society of Chemistry be held responsible for any errors or omissions in this Accepted Manuscript or any consequences arising from the use of any information it contains.

## Efficient selective 4-aminophenol sensing and antibacterial activity of ternary $\text{Ag}_2\text{O}_3 \cdot \text{SnO}_2 \cdot \text{Cr}_2\text{O}_3$ nanoparticles

Md Abdus Subhan<sup>a, e\*</sup>, Sanjida Sultana Jhuma<sup>a</sup>, Pallab Chandra Saha<sup>a</sup>, M. M. Alam<sup>b</sup>,  
Abdullah M. Asiri<sup>c</sup>, Mohammad Al-Mamun<sup>d</sup>, Sara Aly Attia<sup>e</sup>, Tanvir Hossain Emon<sup>f</sup>, Abul  
Kalam Azad<sup>f</sup>, and Mohammed M. Rahman<sup>c,\*</sup>

<sup>a</sup>*Department of Chemistry, School of Physical Sciences, Shah Jalal University of Science and Technology, Sylhet-3114, Bangladesh*

<sup>b</sup>*Department of Chemical Engineering and Polymer Science, Shah Jalal University of Science and Technology, Sylhet 3100, Bangladesh*

<sup>c</sup>*Center of Excellence for Advanced Materials Research & Department of Chemistry, Faculty of Science, King Abdulaziz University, P.O. Box 80203, Jeddah 21589, Saudi Arabia,*

<sup>d</sup>*Center for Clean Environment and Energy, Griffith School of Environment, Gold Coast Campus, Griffith University, QLD 4222, Australia*

<sup>e</sup>*Center for Pharmaceutical Biotechnology and Nanomedicine (CPBN), Department of Pharmaceutical Sciences, Northeastern University, Boston, MA, USA.*

<sup>f</sup>*Department of Genetic Engineering & Biotechnology, Shah Jalal University of Science and Technology, Sylhet-3114, Bangladesh*

(\*Corresponding author's e-mail: [subhan-che@sust.edu](mailto:subhan-che@sust.edu); [mmrahman@kau.edu.sa](mailto:mmrahman@kau.edu.sa))

### **Dr. Md Abdus Subhan**

Professor of the Department of Chemistry  
Shahjalal University of Science and Technology, Sylhet, Bangladesh  
E-mail: [subhan-che@sust.edu](mailto:subhan-che@sust.edu), [md.subhan@northeastern.edu](mailto:md.subhan@northeastern.edu)  
Phone: +8801716073270

**&**

### **Dr. Mohammed M. Rahman,**

Center of Excellence for Advanced Materials Research (CEAMR) &  
Chemistry Department, Faculty of Science, King Abdulaziz University, Jeddah 21589,  
P.O. Box 80203, Saudi Arabia  
Email: [mmrahman@kau.edu.sa](mailto:mmrahman@kau.edu.sa)  
Phone: +966-59-642-1830; Fax: +966-12-695-2292

## Abstract

In this approach,  $\text{Ag}_2\text{O}_3 \cdot \text{SnO}_2 \cdot \text{Cr}_2\text{O}_3$  nanoparticles (NPs) were synthesized by a simple and quick co-precipitation method. The produced materials were characterized by X-ray powder diffraction (XRD), Scanning Electron Microscopy (SEM), Energy-dispersive X-ray spectroscopy (EDS), X-ray photoelectron spectroscopy (XPS), Fourier-transform infrared spectroscopy (FTIR), and Photoluminescence (PL). Hydrodynamic size and zeta potential were observed in acidic and basic pH. Photocatalytic activities of the newly synthesized composite were studied considering various parameters. Antibacterial activity tests showed  $\text{Ag}_2\text{O}_3 \cdot \text{SnO}_2 \cdot \text{Cr}_2\text{O}_3$  is an excellent anti-bacterial agent. A consistent electrochemical sensor probe was designed by the synthesized  $\text{Ag}_2\text{O}_3 \cdot \text{SnO}_2 \cdot \text{Cr}_2\text{O}_3$  NPs onto the flat part of GCE, which showed an excellent oxidation activity towards the selective 4-aminophenol (4-AP) in phosphate buffer medium. During the electrochemical analysis, the desired 4-AP sensor was found to response linearly over the large concentration range (0.1 nM~0.01 mM) known as linear dynamic range (LDR) and exhibited appreciable sensitivity ( $25.1962 \mu\text{A} \mu\text{M}^{-1} \text{cm}^{-2}$ ). Furthermore, it was showed that the considerably lower limit of detection ( $98.41 \pm 4.92 \text{ pM}$ ), good reproducibility, fast response (20.0 sec.), and long-term stability in phosphate buffer medium. This is an efficient method for the fabrication of selective electrochemical sensor by the electrochemical approach for the safety of environmental and healthcare fields.

**Keywords:**  $\text{Ag}_2\text{O}_3 \cdot \text{SnO}_2 \cdot \text{Cr}_2\text{O}_3$  nanoparticles; Photo-catalysis; Antibacterial activity; Electrochemical sensor development; 4-aminophenol; Environmental safety.

## 1. Introduction

Nanostructured mixed metal oxides play a very important role due to their versatile technological applications and outstanding properties.<sup>1-5</sup> Depending on the size, structure and morphology of the nanoparticles, their magnetic, optical, catalytic and electronic properties vary. Thus, the nanosized particles exhibit a relatively higher performance compared to the bulk materials due to the changes of semiconductor band structure.<sup>6</sup> The multiphase nanocomposite based on two or more different metal oxides coexisting in the same matrix could pose the modified properties due to the metal-metal and metal-oxygen interactions.<sup>7</sup> By the development of new composite material could open up a new dimension for research and applications. The numerous methods are involved for the preparation of the mixed metal oxides including sol-gel,<sup>8,9</sup> wet impregnation,<sup>10</sup> mechanochemical synthesis,<sup>11</sup> hydrothermal method,<sup>12,13</sup> sonochemical, co-precipitation,<sup>14,15</sup> electrochemical,<sup>16</sup> and pyrolysis<sup>17,18</sup>.

The tin oxide (SnO<sub>2</sub>) is a semiconductor material with the band gap energy of 3.6 eV and has the wider technological applications including transistors, electrodes, liquid crystal displays, catalysts, photovoltaic devices, electrochemical sensors, and antistatic coating.<sup>19-23</sup> As the electrochemical sensor in I-V approach, SnO<sub>2</sub> is extensively applied to detect the environmental toxic chemicals such as acetone,<sup>24,25</sup> and Benzaldehyde<sup>26</sup>. The silver (Ag) is a noble metal and prominent in the field of the nanomaterial research, due to its unique properties such as sensing, optoelectronic and catalytic, feasible to apply in the various technological fields<sup>27</sup> including high temperature resistant materials,<sup>28</sup> corrosive resistant materials,<sup>29</sup> liquid crystal display,<sup>30,31</sup> green pigment,<sup>32</sup> catalyst<sup>33,34</sup> and so on. Specifically, the silver oxide has been reported as a sensor to detect various environmental toxic chemicals in electrochemical (I-V) approach.<sup>35-37</sup> In this study, the special attention has been focused on the formation and the properties of chromium (III) oxide (Cr<sub>2</sub>O<sub>3</sub>) among the different stable oxidation states of its. Due to its high stability and

1  
2  
3 electrochemical activity, it has been applied as a sensing material for the fabrication of  
4 electrochemical sensor to detect various chemicals and biochemical.<sup>38,39</sup> By the mixing of three  
5 different oxides in the matrix, a new nanocomposite of  $\text{Ag}_2\text{O}_3 \cdot \text{SnO}_2 \cdot \text{Cr}_2\text{O}_3$  is formed, which  
6 shows the deferent physical and electrochemical properties rather than the individual ones and  
7 the co-precipitation method has been applied to prepare this ternary metal oxide. This method for  
8 the preparation of the nanocomposite metal oxides is famous, due to easy operation, economical,  
9 versatile, promising scale-up synthesis and effective for large scale production.<sup>40</sup> This composite  
10 has been characterized and the various applications have been studied. The most fascinating  
11 applications of this nanocomposite as a photocatalyst to degrade the organic dye released by  
12 textile and dyeing industries, which is burning issue nowadays due to the cause of pernicious  
13 effect both human life and environment.<sup>41</sup> Optical properties and antibacterial activities of the  
14 synthesized nanocomposite also have been studied.

15  
16  
17  
18  
19  
20  
21 As the major ingredient for the formulation of paracetamol, the 4-aminophenol (4-AP) is  
22 used as a drug to the relief of the fever and the pain associated with arthritis, backache, headache,  
23 and postoperative pains. The 4-AP in the paracetamol is available in the form of syrups,  
24 suspension, tablets and injections in the drug market depending on the patient's requirement such  
25 as pregnant women, children, and elderly people. Due to the accumulation of 4-AP in human  
26 through the intake of paracetamol may cause numerous pathological syndromes such as  
27 hepatotoxicity and nephrotoxicity.<sup>42-45</sup> Therefore, considering the toxicity of 4-AP, it has been  
28 restricted to 50 ppm as the maximum concentration in the formulation of paracetamol by  
29 European Union and USA.<sup>46,47</sup> Besides this, as a base industrial raw material, 4-AP is used  
30 extensively to produce various chemicals such as inhibitor, dyestuff, petroleum additives and  
31 developer.<sup>48</sup> As it is stated that 4-AP has a hazardous effect on both human and environment.  
32  
33  
34  
35  
36  
37  
38  
39  
40  
41  
42  
43  
44  
45  
46  
47  
48  
49  
50  
51  
52  
53  
54  
55  
56  
57  
58  
59  
60

Therefore, it is a necessity to the development of sensitive and reliable methods for the detection of 4-AP. Up to date, the numerous conventional analytical methods are applying to detect 4-AP such as capillary electrophoresis,<sup>49,50</sup> electrochemical detection,<sup>51</sup> high-performance liquid chromatography (HPLC) coupled with UV-visible,<sup>52,53</sup> fluorescence<sup>54</sup> and flow-based analytical techniques<sup>55,56</sup>. But these methods are limited due to various drawbacks such heavy and costly instruments, expensive analyzing reagents, time-consuming and non-portable. On the other hand, the electrochemical methods are sensitive, quick detection time, inexpensive with in-situ detection facilities, simple and easy detection methods. A number of researches based on various metal oxides or nanocomposites by electrochemical approach have been reported to detect the various environmental toxicants, chemicals and biochemical and reported elsewhere.<sup>57-61</sup> Furthermore, the electrochemical method particularly I-V approach becoming popular and the regarding this, a number of researches based on the various oxides of transition metals as sensing mediators have reported recently to detect numerous toxic chemicals and biochemicals<sup>62-71</sup>. This study will be performed to develop an electrochemical sensor in electrochemical approach using  $\text{Ag}_2\text{O}_3 \cdot \text{SnO}_2 \cdot \text{Cr}_2\text{O}_3$  NPs onto GCE.

As an essential part of this study, the synthesized  $\text{Ag}_2\text{O}_3 \cdot \text{SnO}_2 \cdot \text{Cr}_2\text{O}_3$  NPs was deposited onto the GCE as the thin uniform layer with conductive nafion (5% suspension in ethanol) to develop the desire working electrode for the chemical sensor selective to 4-AP. A calibration curve was plotted using current vs. concentration of 4-AP relation and identifying the linear region in the calibration curve, where the linear dynamic range (LDR) was labeled. The sensitivity of the proposed 4-AP chemical sensor was calculated from the slope of the calibration curve by considering the active surface area of GCE ( $0.0316 \text{ cm}^2$ ). The detection limit was also computed from the slope of the calibration curve by considering the signal to noise ratio of 3.

## 2. Experimental

### 2.1 Materials and methods

All the chemicals used for this research purpose including silver nitrate (Sigma Aldrich, Germany), tin chloride hydrate (Merck, Germany), chromium chloride hexahydrate (Sigma Aldrich), acetone (Merck, Germany), sodium carbonate (AR, BDH) were purchased. As the requirement of this study, the toxic chemicals in the form of analytical grade such as 2-aminophenol (2-AP), 3-methoxyphenol (3-MP), 4-aminophenol (4-AP), 4-hexylresorcinol, melamine, m-tolyl hydrazine hydrochloride (M-THyHCl), phenylhydrazine (PHyd), zimaldehyd were obtained from a local supplier of Sigma-Andrich. The auxiliary reagents including monosodium, disodium phosphate buffer, concentrated liquid ammonia and a conductive binding agent (5% nafion suspension in ethanol) were used. Double beam UV-Visible spectrophotometer (UV-1800 series, UV-Vis Spectrophotometer, Shimadzu Corporation, Kyoto, Japan) was used for the measurement of absorbance. Quartz cells of 1 cm path were used as a sample holder. For PL study Spectrofluorometer (Shimadzu Corporation, Kyoto, Japan) was used. For calcination, electric muffle furnace was used. FTIR spectrophotometer (Shimadzu, IRPrestige-21) was used in this work. Bulk crystal phase identification and other structural information of the materials studied in this work were characterized by X-ray diffraction (XRD, Bruker D8 Advance diffractometer, equipped with a graphite monochromator). The diffraction patterns were recorded in the step scan mode at 0.05 steps and the measurement rate of 10 s/step. The diffraction patterns were registered within the  $2\theta$  angle range from  $10^\circ$  to  $80^\circ$ . The surface morphology and nanostructure characterizations were performed by using a Scanning Electron Microscope (SEM) equipped with an Energy-Dispersive X-ray Spectrometer (EDS) (JSM-7100F) linked with an EDS (Oxford) mapping device. XPS investigation was performed for nanomaterials using a K- $\alpha$ 1 spectrometer (Thermo scientific, K- $\alpha$ 1 1066) with an excitation

1  
2  
3 radiation source (Al K $\alpha$ 1, Beam spot size = 300.0  $\mu$ m, pass energy = 200.0 eV, pressure 10<sup>-8</sup>  
4 torr). Hydrodynamic size and zeta potential were measured by Zetasizer Nanoseries (Nano-  
5 ZS90). The Ag<sub>2</sub>O<sub>3</sub>·SnO<sub>2</sub>·Cr<sub>2</sub>O<sub>3</sub> nanoparticle modified GCE electrode served as a working  
6 electrode, whereas an Ag/AgCl (sat. KCl) and a Pt wire acted as a reference and counter  
7 electrodes, respectively. All the electrochemical experiments were conducted in 0.1 M phosphate  
8 buffer solution (PBS) under N<sub>2</sub> atmosphere condition, where the volume of solution was 10 ml.  
9 The Ag<sub>2</sub>O<sub>3</sub>·SnO<sub>2</sub>·Cr<sub>2</sub>O<sub>3</sub> nanoparticle was characterized by means of electrochemical impedance  
10 spectroscopy (EIS). The Keithly electrometer was used to the assembled the desire  
11 electrochemical (sensor) cell.

## 2.2 Synthesized of Ag<sub>2</sub>O<sub>3</sub>·SnO<sub>2</sub>·Cr<sub>2</sub>O<sub>3</sub> NPs

12  
13  
14  
15  
16  
17  
18  
19  
20  
21  
22  
23  
24  
25  
26  
27  
28  
29  
30  
31  
32  
33  
34  
35  
36  
37  
38  
39  
40  
41  
42  
43  
44  
45  
46  
47  
48  
49  
50  
51  
52  
53  
54  
55  
56  
57  
58  
59  
60

The composite Ag<sub>2</sub>O<sub>3</sub>·SnO<sub>2</sub>·Cr<sub>2</sub>O<sub>3</sub> was prepared by co-precipitation method from their salts as precursors. At first solutions of 0.25 M, 20 mL of AgNO<sub>3</sub> (0.849 gm), SnCl<sub>2</sub>·2H<sub>2</sub>O (1.128 gm), CrCl<sub>3</sub>·6H<sub>2</sub>O (1.332 gm) respectively and solution of 1.0 M Na<sub>2</sub>CO<sub>3</sub> were prepared by using distilled water. Then the solutions were mixed together in a beaker in 1:1:1 ratio and stirred vigorously at room temperature for 5 minutes. Then the solution of 1.0 M Na<sub>2</sub>CO<sub>3</sub> was added slowly with agitation until precipitation was complete. The resultant mixture was stirred for a further 4 hours at 45 °C with constant stirring. Then white metal carbonate precipitates were separated from the solution by centrifugation, washed several times with deionized water and finally dried at 150 °C for two hours in an oven. The obtained white precipitate was calcined in a muffle furnace at 600 °C and 850 °C for five hours respectively. Oxides are formed from their carbonates by calcination.

## 2.3 The fabrication of GCE working electrode using Ag<sub>2</sub>O<sub>3</sub>·SnO<sub>2</sub>·Cr<sub>2</sub>O<sub>3</sub> NPs

The fabrication of a working electrode of the proposed electrochemical sensor by using  $\text{Ag}_2\text{O}_3 \cdot \text{SnO}_2 \cdot \text{Cr}_2\text{O}_3$  NPs onto flat GCE is an essential part of this study. For this reason, the thinner film with active  $\text{Ag}_2\text{O}_3 \cdot \text{SnO}_2 \cdot \text{Cr}_2\text{O}_3$  NPs in ethanol was prepared to make the thin uniform-layer onto GCE. Then, the modified GCE with  $\text{Ag}_2\text{O}_3 \cdot \text{SnO}_2 \cdot \text{Cr}_2\text{O}_3$  NPs was kept at ambient conditions to completely dry. After that, a drop of nafion (the nafion commercially available as 5% suspension in ethanol and known as a conductive binding agent) was added on the modified GCE to enhance the stability of the NPs on GCE during the electrochemical analysis in phosphate buffer medium. When the Nafion is dropped onto the  $\text{Ag}_2\text{O}_3 \cdot \text{SnO}_2 \cdot \text{Cr}_2\text{O}_3$  NPs coated GCE, it is soaked the coated nanomaterials homogeneously and distributed throughout coated-film. When it is dried at 35 °C inside an oven for an hour, a homogeneous thin-film is resulted to form onto the GCE by  $\text{Ag}_2\text{O}_3 \cdot \text{SnO}_2 \cdot \text{Cr}_2\text{O}_3$  NPs. To assemble the electrochemical (sensor) cell, the modified GCE and a simple Pt-wire were connected in a series with the Keithly electrometer. The resulted electrochemical sensor is based on two electrodes system, where the connected modified GCE is functioned as working and the Pt-wire as counter electrode respectively. The 4-AP was diluted in the deionized water to form several solutions based on concentration ranging in the sequence from 0.1 mM to 0.1 nM. During the electrochemical investigation, the sensor analytical performances such as sensitivity, linear dynamic range, detection limit, reproducibility, stability and response time were measured at ambient conditions. The phosphate buffer solution was taken in the investigating beaker as 10.0 mL as constant through the electrochemical analysis.

### 3. Results and discussion

#### 3.1 Structural Analysis of $\text{Ag}_2\text{O}_3 \cdot \text{SnO}_2 \cdot \text{Cr}_2\text{O}_3$ nanoparticles

As shown in Fig. 1,  $2\theta$  peaks observed at  $26.579^\circ$ ,  $33.864^\circ$ ,  $37.941^\circ$ ,  $38.965^\circ$ ,  $42.625^\circ$ ,  $51.756^\circ$ ,  $57.804^\circ$ ,  $61.861^\circ$ ,  $64.714^\circ$ ,  $65.943^\circ$ ,  $71.754^\circ$ , and  $78.68^\circ$  are due to tetragonal  $\text{SnO}_2$  (Cassiterite). The diffraction peaks of  $\text{SnO}_2$  was detected in the sample, can be indexed to (hkl) values of (110), (101), (200), (111), (210), (211), (002), (310), (112), (301), (911), and (321) diffraction planes. Peaks are confirmed by matching with PDF file number 99-0024 (Intensity matching 91%). Similarly, the presence of orthorhombic silver oxide ( $\text{Ag}_2\text{O}_3$ ) in this nanoparticle can be identified by the  $2\theta$  peaks at  $26.665^\circ$ ,  $27.705^\circ$ ,  $33.246^\circ$ ,  $36.16^\circ$ ,  $41.405^\circ$ ,  $43.807^\circ$ ,  $45.508^\circ$ ,  $51.849^\circ$ ,  $52.897^\circ$ ,  $54.724^\circ$ ,  $57.22^\circ$ ,  $60.19^\circ$ ,  $62.428^\circ$ ,  $69.278^\circ$ ,  $71.312^\circ$  and  $76.458^\circ$  (PDF file number 77-1829, Intensity matching 52%). Diffraction peaks of  $\text{Ag}_2\text{O}_3$  was detected in (110), (400), (101), (131), (331), (511), (620), (211), (022), (351), (800), (622), (911), (280), and (321) diffraction planes. Finally, rhombohedral chromium oxide ( $\text{Cr}_2\text{O}_3$ ) can be detected in (101), (131), (222), (020), (220), (351), (130), (230), (342), (241), and (330) diffraction planes by  $2\theta$  values at  $33.606^\circ$ ,  $36.192^\circ$ ,  $39.765^\circ$ ,  $44.191^\circ$ ,  $50.215^\circ$ ,  $54.85^\circ$ ,  $63.451^\circ$ ,  $65.094^\circ$ ,  $73.348^\circ$ ,  $76.81^\circ$ , and  $79.059^\circ$  (PDF file number 85-0730, intensity matching 34%). The deviation (observed by Intensity Matching) from the XRD patterns of individual oxides were calculated using Jade MDI software and could be due to the synergic effect involved in mixing three different metal oxides to form tri-metallic oxide. Hence, the nanocomposite might possess different characteristics than its corresponding individual oxides. The particle size of the nanocomposite was estimated from XRD data to be 34.6 nm using Scherrer's formula  $\tau = K\lambda/(\beta\cos\theta)$ . Where  $\tau$  is the mean size,  $K$  is a dimensionless shape factor with a value 0.94,  $\lambda$  is the x-ray wavelength (0.1506 nm),  $\beta$  is the line broadening at half the maximum intensity (FWHM) and  $\theta$  is the Bragg angle.

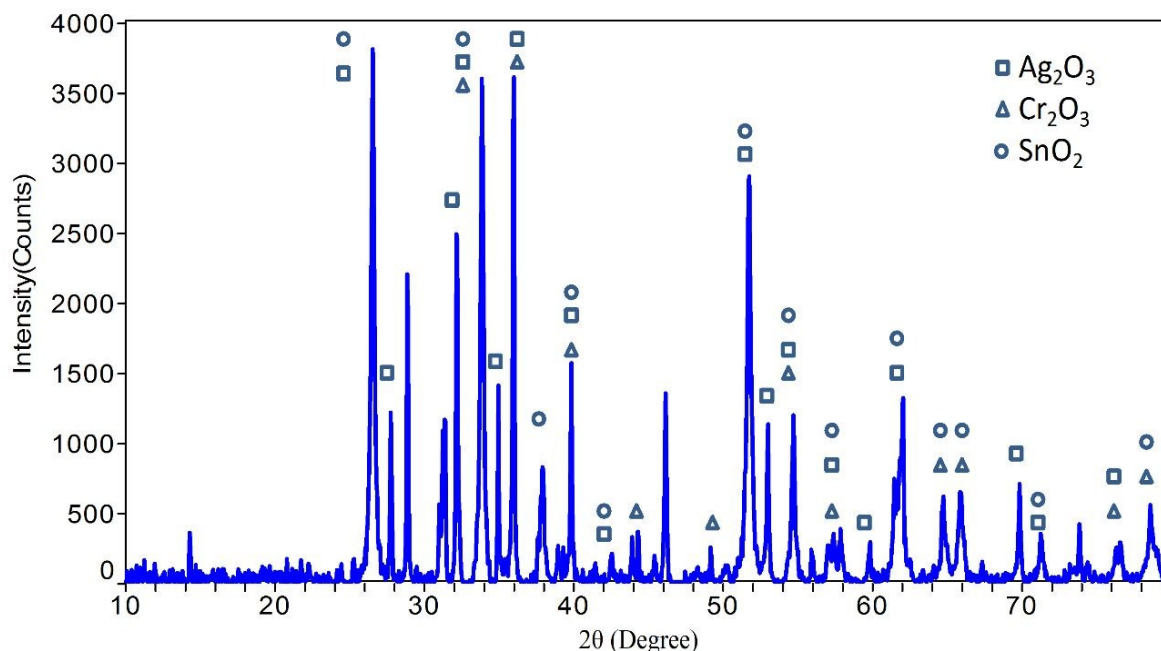


**Fig. 1** X-Ray powder diffraction pattern of  $\text{Ag}_2\text{O}_3 \cdot \text{SnO}_2 \cdot \text{Cr}_2\text{O}_3$  nanoparticles

### 3.2 Surface analysis of $\text{Ag}_2\text{O}_3 \cdot \text{SnO}_2 \cdot \text{Cr}_2\text{O}_3$ nanoparticle

The SEM images in Fig. 2 revealed the morphology of  $\text{Ag}_2\text{O}_3 \cdot \text{SnO}_2 \cdot \text{Cr}_2\text{O}_3$  nanoparticles. The nanoparticles formed irregular morphology with combination of three different oxides in the matrix, which might have high surface activity, resulting in perhaps higher catalytic and sensor activity. Fig 2 shows different morphologies of the particles on the surface.

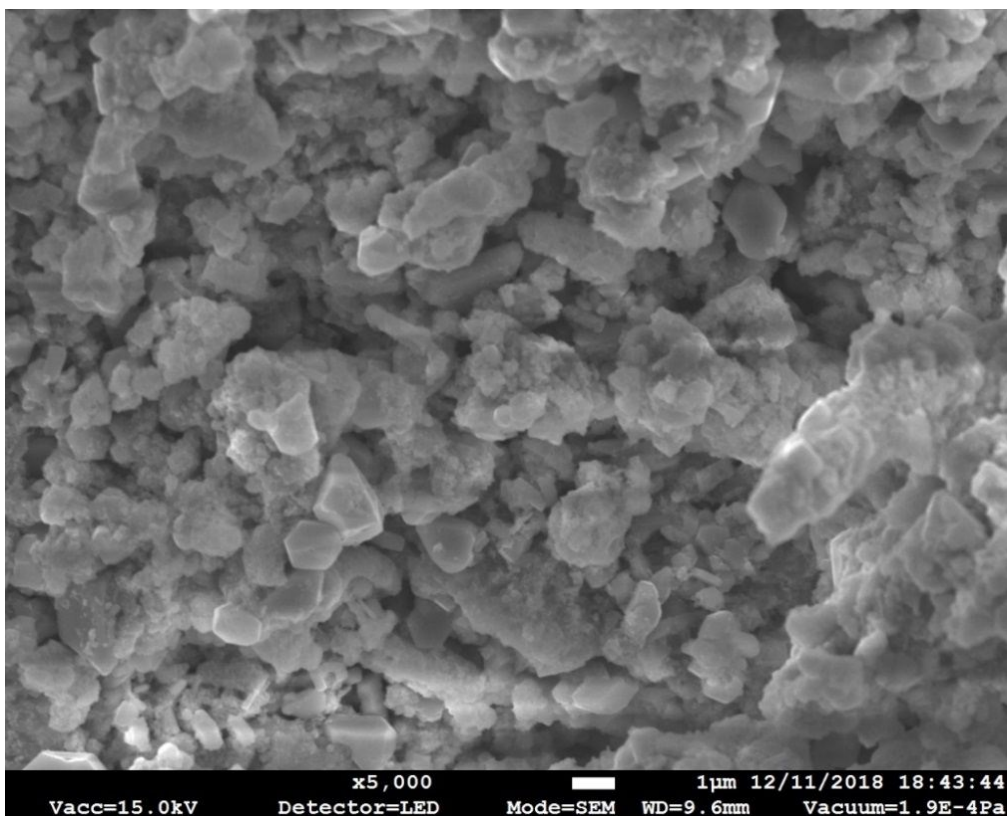


**Fig. 2** SEM image of  $\text{Ag}_2\text{O}_3 \cdot \text{SnO}_2 \cdot \text{Cr}_2\text{O}_3$  nanoparticle

### 3.3 Qualitative Analysis of $\text{Ag}_2\text{O}_3 \cdot \text{SnO}_2 \cdot \text{Cr}_2\text{O}_3$ nanoparticle

The EDS study was carried out to map the elemental composition as well as the distribution of the elements in the nanoparticle matrix (Figure 3). As is evident from **Table 1**, the NPs are composed of Sn, Ag, Cr, and O with an atomic percentage of 13.98%, 18.21%, 15.28%, and 52.54%.

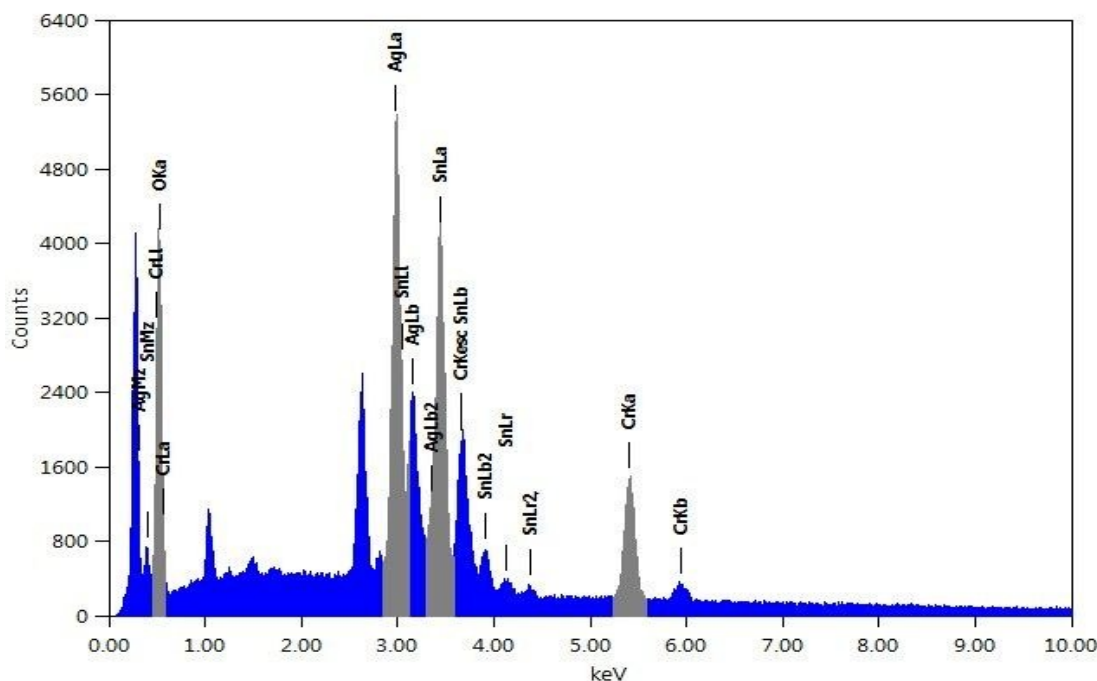


**Fig. 3** EDS spectrum of  $\text{Ag}_2\text{O}_3 \cdot \text{SnO}_2 \cdot \text{Cr}_2\text{O}_3$  nanoparticle

**Table 1.** Elemental Analysis of  $\text{Ag}_2\text{O}_3 \cdot \text{SnO}_2 \cdot \text{Cr}_2\text{O}_3$  nanoparticle

Element	(keV)	Mass%	Atom%
O K	0.525	15.99	52.54
Cr K	5.411	15.1	15.28
Ag L	2.983	37.36	18.21
Sn L	3.442	31.55	13.98
<b>Total</b>		100	100

### 3.4 XPS analysis of $\text{Ag}_2\text{O}_3 \cdot \text{SnO}_2 \cdot \text{Cr}_2\text{O}_3$ nanoparticle

Fig. 4 shows the XPS spectrum of  $\text{Ag}_2\text{O}_3 \cdot \text{SnO}_2 \cdot \text{Cr}_2\text{O}_3$  NPs. XPS peaks are observed corresponding to nano  $\text{Ag}_2\text{O}_3$ ,  $\text{Cr}_2\text{O}_3$ ,  $\text{SnO}_2$  in mixed metal nanoparticle oxide in  $\text{Ag}_2\text{O}_3 \cdot \text{Cr}_2\text{O}_3 \cdot \text{SnO}_2$ . Peaks are assigned at different binding energies (eV) for each metal in metal oxides from lower energy to higher energy, Sn( $3d_{5/2}$ ), Sn( $3d_{3/2}$ ), Sn(3p<sub>3</sub>), Cr(3p<sub>3/2</sub>), Sn(3p<sub>1</sub>), Sn(3s), Ag(3d<sub>3/2</sub>), Ag(3p<sub>5/2</sub>), Cr(2p<sub>1/2</sub>), and Sn(4d). The XPS results clearly indicated the formation of mixed metal nanoparticle oxide in  $\text{Ag}_2\text{O}_3 \cdot \text{SnO}_2 \cdot \text{Cr}_2\text{O}_3$ .

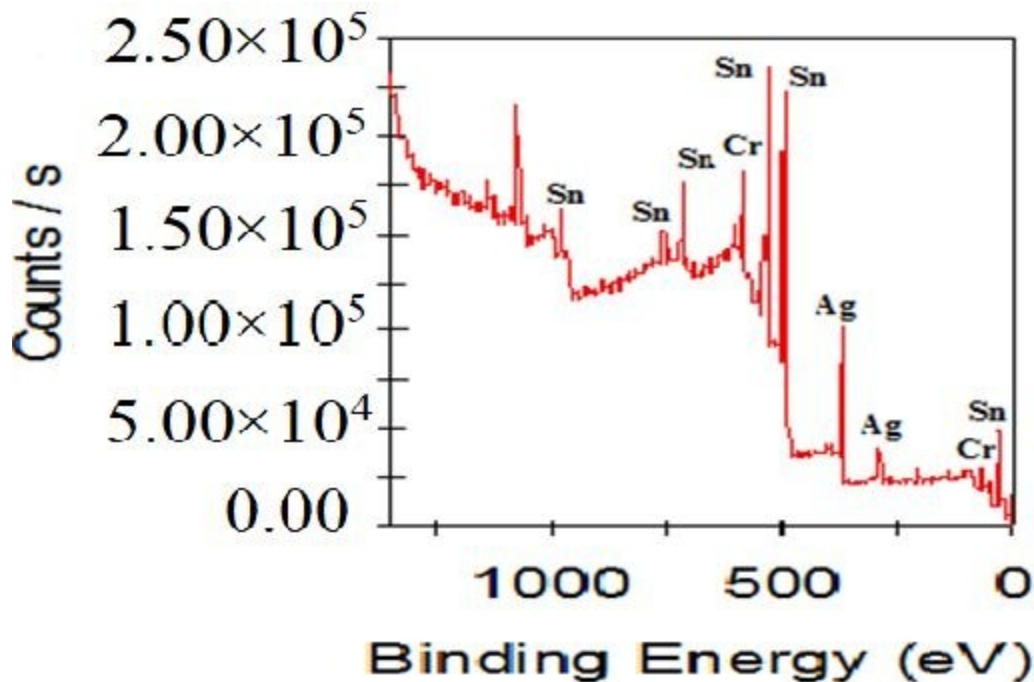


**Fig. 4** XPS spectrum of  $\text{Ag}_2\text{O}_3 \cdot \text{SnO}_2 \cdot \text{Cr}_2\text{O}_3$  nanoparticle

### 3.5 FTIR analysis of $\text{Ag}_2\text{O}_3 \cdot \text{SnO}_2 \cdot \text{Cr}_2\text{O}_3$ nanoparticle

In the FTIR spectrum (Fig. S1) of  $\text{Ag}_2\text{O}_3 \cdot \text{SnO}_2 \cdot \text{Cr}_2\text{O}_3$  nanoparticle, peaks are observed in the region of 400-1000  $\text{cm}^{-1}$  correspond to the vibration modes of M-O and M-O-M (M = Ag, Cr, Sn). IR band at 3358.07  $\text{cm}^{-1}$  due to the stretching mode of O-H group indicates the presence of absorbed water. IR peak observed at 943.19  $\text{cm}^{-1}$  may be assigned to Sn-O, peak at 855.33  $\text{cm}^{-1}$  is due to Cr-O low frequency vibration. Peaks observed at 690.5 and 503.42  $\text{cm}^{-1}$  are assigned to Ag-O vibrations.

### 3.6 Zeta potential and hydrodynamic size of $\text{Ag}_2\text{O}_3 \cdot \text{SnO}_2 \cdot \text{Cr}_2\text{O}_3$ nanocomposite

Zeta potential and hydrodynamic size of  $\text{Ag}_2\text{O}_3 \cdot \text{SnO}_2 \cdot \text{Cr}_2\text{O}_3$  nanocomposite were studied both in acidic (Na-citrate buffer) and basic (PBS buffer) pH at 25 °C to know the size and charge in dispersed media. Hydrodynamic size, zeta potential and poly dispersive index (PDI) have been listed in Table 2. The hydrodynamic size of  $\text{Ag}_2\text{O}_3 \cdot \text{SnO}_2 \cdot \text{Cr}_2\text{O}_3$  in acidic pH and basic pH was found to be 1113.5 and 1174 nm respectively. Zeta potential in acidic and basic pH has been

observed to be -27.05 and -26.2 mV respectively. The results indicated that  $\text{Ag}_2\text{O}_3 \cdot \text{SnO}_2 \cdot \text{Cr}_2\text{O}_3$  particles are negatively charged and can easily adsorb organic compounds, dyes and organic chemical toxins on the particle surface either in acidic or basic media and perform catalytic functions. Observation of single peak with 100% intensity during the measurement of the hydrodynamic size designated the formation of a single particle by the mixing of individual oxides  $\text{Ag}_2\text{O}_3$ ,  $\text{SnO}_2$  and  $\text{Cr}_2\text{O}_3$ . Detailed structural investigations will provide further insight into it.

**Table 2.** Hydrodynamic size and zeta potential of  $\text{Ag}_2\text{O}_3 \cdot \text{SnO}_2 \cdot \text{Cr}_2\text{O}_3$

Nanocomposite	Na-citrate buffer (pH 4.95)			PBS buffer (pH 7.4)		
	Size (nm)	Zeta potential (mV)	PDI	Size (nm)	Zeta potential (mV)	PDI
$\text{Ag}_2\text{O}_3 \cdot \text{SnO}_2 \cdot \text{Cr}_2\text{O}_3$	1113.5	-27.05	0.190	1174.0	-26.20	0.191

### 3.7 UV-Visible spectrum and band gap determination of $\text{Ag}_2\text{O}_3 \cdot \text{SnO}_2 \cdot \text{Cr}_2\text{O}_3$ nanocomposite

The absorption spectrum of  $\text{Ag}_2\text{O}_3 \cdot \text{SnO}_2 \cdot \text{Cr}_2\text{O}_3$  nanocomposite dispersed in acetone solution and band-gap determined from the UV-Visible spectra are shown in **Fig. 5**. It was found that a broad diffusion peak is observed in the UV region at 349 nm. The UV-Visible spectral study may be assisted in understanding the electronic structure of the optical band gap of the material. Absorption in the near ultraviolet region arises from electronic transitions associated within the sample.

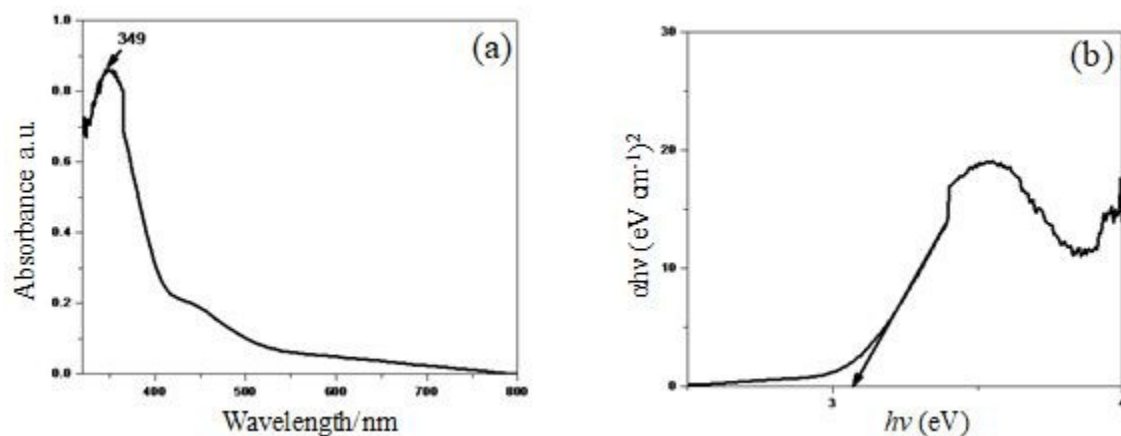


Fig. 5

Figure 5. (a) UV – Visible spectrum and (b) band gap of  $\text{Ag}_2\text{O}_3 \cdot \text{Cr}_2\text{O}_3 \cdot \text{SnO}_2$  nanocomposite

The optical band gap of the produced nanocomposite is calculated using the Tauc's equation

$$(\alpha h\nu)^2 = A(h\nu - E_g)$$

where  $\alpha$  is an absorption coefficient,  $h\nu$  is the photon energy ( $h$  is the Planck's constant and  $\nu$  is the photon frequency),  $E_g$  is the optical band gap and  $A$  is a constant usually taken as unity. The band gap is found by plotting  $(\alpha h\nu)^2$  against  $h\nu$ . The value of the band gap is determined by the intercept of the straight line at  $\alpha = 0$ . Since the band gap of  $\text{Ag}_2\text{O}_3 \cdot \text{Cr}_2\text{O}_3 \cdot \text{SnO}_2$  is 3.06 eV. The nanocomposite is able to absorb UV and visible light and may show good photocatalytic activity.

### 3.8 Study of PL property $\text{Ag}_2\text{O}_3 \cdot \text{SnO}_2 \cdot \text{Cr}_2\text{O}_3$ nanoparticle

PL spectra of  $\text{Ag}_2\text{O}_3 \cdot \text{SnO}_2 \cdot \text{Cr}_2\text{O}_3$  nanoparticle annealed at 600 °C (as shown in Fig. 6(a)) and 850 °C (Fig. 6(b)) were measured at room temperature in acetone at different excitation wavelengths. Two emission peaks at 436 nm and 467 nm were observed when it was excited at 320 nm in case of composite annealed at 600 °C. When the sample was excited at 350 nm emission peaks were observed at 431 nm and 466 nm. Emission peaks at 426 nm and 464 nm were observed at excitation wavelength 370 nm. Excitation at 380 nm provided emissions at 427 nm and 462 nm. Emissions in the visible region ranging from 420-470 nm indicate blue band.<sup>72</sup> The broad blue emission band might arise from the ionized oxygen vacancies to the valence

band. Due to the radiative recombination of a photogenerated hole with an electron occupying the oxygen vacancies the blue emission is observed.<sup>73</sup> The structured emission peaks from 420-470 nm resembles emission from d-d states of chromium ions in octahedral molecular complexes. The chromium ions in Cr<sub>2</sub>O<sub>3</sub> are also in octahedral coordination sites and the structured emission may be originated from the Cr d-d states. The emission data is compiled in Table S1.

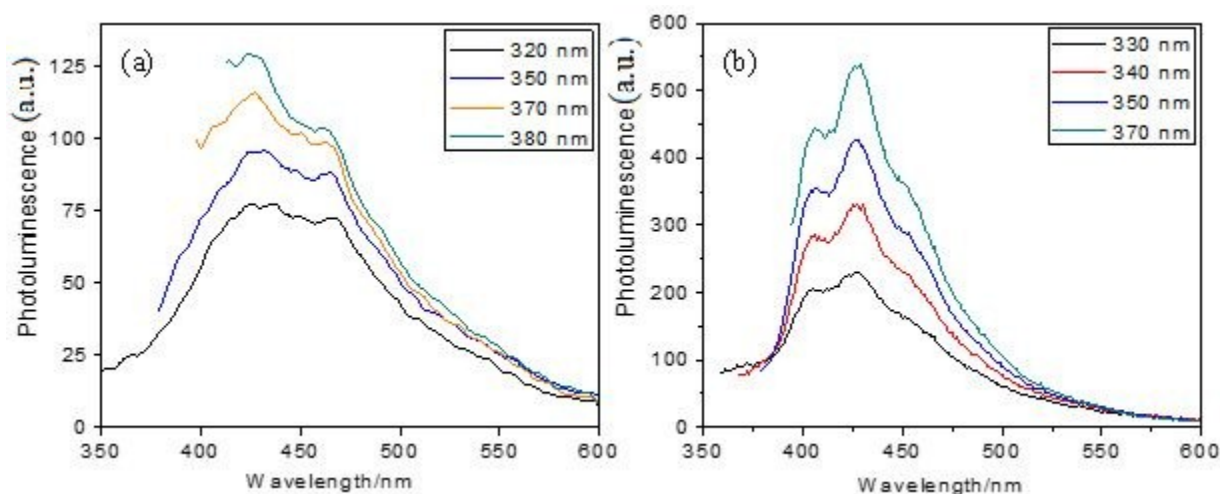


**Fig. 6** PL spectra of Ag<sub>2</sub>O<sub>3</sub>·SnO<sub>2</sub>·Cr<sub>2</sub>O<sub>3</sub> nanoparticles annealed (a) at 600 °C and (b) at 800 °C.

Similarly, three emission peaks at 403, 426 and 454 nm can be found when excited the 800 °C annealed composite with 330 nm energy. In the same way, peaks with three maxima and different intensity were found when the nanoparticle was excited with 340 nm (404, 427 and 453 nm emissions), 350 nm (405, 426 and 452 nm emissions) and 370 nm (405, 428 and 454 nm emissions). The emission energy is listed in Table S2.

### 3.9 Study of Photocatalytic activity of Ag<sub>2</sub>O<sub>3</sub>·SnO<sub>2</sub>·Cr<sub>2</sub>O<sub>3</sub> nanoparticle

To examine the photocatalytic activity of Ag<sub>2</sub>O<sub>3</sub>·SnO<sub>2</sub>·Cr<sub>2</sub>O<sub>3</sub> nanoparticles an aqueous solution of methyl violet 6b (MV) dye was irradiated with 200 W tungsten lamp. A certain amount of photocatalyst was added to the methyl violet (6b) dye solution in a beaker which was

1  
2  
3 stirred for 1.0 h prior to irradiation to ensure adsorption-desorption equilibrium. 4.0 ml of dye  
4 solutions were separated from the photocatalyst to record the changes of dye concentration at  
5 regular gaps which were observed spectrophotometrically. The degradation was performed at pH  
6 9 and pH 7 in the presence of photocatalyst under different conditions. Spectrophotometric  
7 measurement evaluates degradation of MV dye as a function of time and it was observed that the  
8 absorption intensity of MV dye decreases with increasing time in the presence of photocatalyst.  
9 The following equation was used to calculate the photocatalytic efficiency  $\eta$ .

$$\text{Photocatalytic efficiency } \eta = (1-C/C_0) \times 100 = (1-A/A_0) \times 100$$

10  
11  
12  
13  
14  
15  
16  
17  
18  
19  
20  
21  
22  
23  
24  
25  
26  
27  
28  
29  
30  
31  
32  
33  
34  
35  
36  
37  
38  
39  
40  
41  
42  
43  
44  
45  
46  
47  
48  
49  
50  
51  
52  
53  
54  
55  
56  
57  
58  
59  
60  
Where  $C_0$  denotes the concentration of MV before irradiation and  $C$  is the concentration of irradiation time,  $A$  and  $A_0$  are the corresponding absorbances.

### 3.10 Effect of photocatalytic amount of $\text{Ag}_2\text{O}_3 \cdot \text{SnO}_2 \cdot \text{Cr}_2\text{O}_3$ nanoparticle on photo-degradation

At first, to determine the effective dose for studying the photocatalytic activity of  $\text{Ag}_2\text{O}_3 \cdot \text{SnO}_2 \cdot \text{Cr}_2\text{O}_3$  various amounts of photocatalyst were taken to examine the effect of photocatalyst dose on dye degradation under visible light irradiation as shown in Fig. 7. Several amounts of photocatalyst ranging from  $0.03 \text{ gL}^{-1}$  to  $0.06 \text{ gL}^{-1}$  MV solutions were taken in this study. With increasing photocatalyst amount degradation percentages of MV were gradually increased and the highest degradation was observed in case of  $0.05 \text{ gL}^{-1}$  (77.88%, 95.89%, 99% and 87% for  $0.03 \text{ gL}^{-1}$ ,  $0.04 \text{ gL}^{-1}$ ,  $0.05 \text{ gL}^{-1}$  and  $0.06 \text{ gL}^{-1}$ , respectively). After reaching the highest peak for optimum dosage  $0.05 \text{ gL}^{-1}$  the efficiency began to fall.

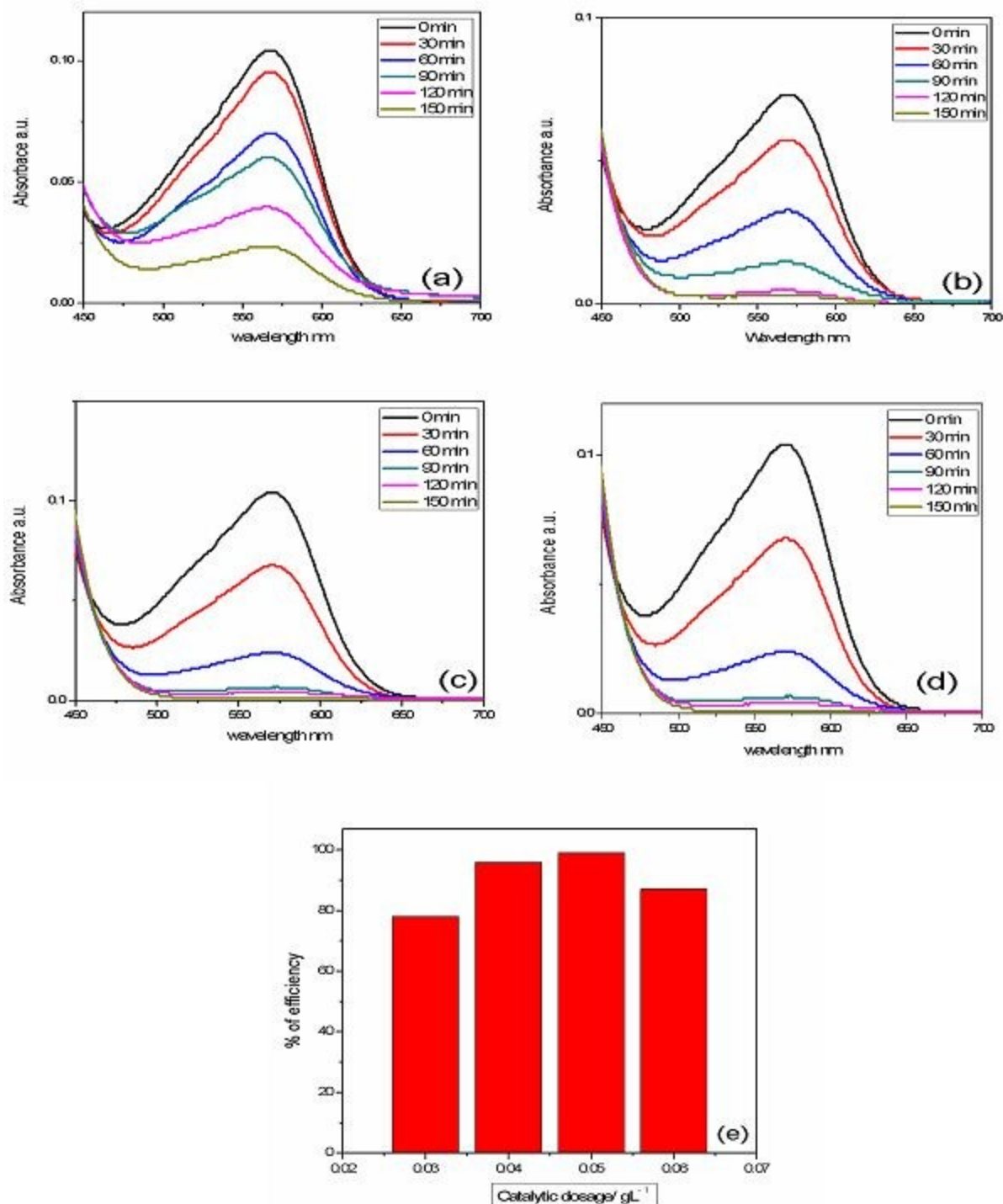


**Fig. 7** Effect of catalyst amount on degradation rate constants of MV under visible light, (a) 0.03 gL<sup>-1</sup>; (b) 0.04 gL<sup>-1</sup>; (c) 0.05 gL<sup>-1</sup>; (d) 0.06 gL<sup>-1</sup> dosage; degradation of MV (MV concentration:

1  
2  
3 50 ppm; pH 9; irradiation time: 150 min) and (e) represents compiled percent of degradation  
4 efficiency at different dose(a-d) of nanocomposite.  
5  
6

7  
8  
9 A 5.0 mg of photo-catalyst was added to the methyl violet (6b) dye solution in a beaker  
10 (100 ml solution) which was stirred for 1 h prior to irradiation for studying the photocatalytic  
11 activity of  $\text{Ag}_2\text{O}_3 \cdot \text{SnO}_2 \cdot \text{Cr}_2\text{O}_3$ . As shown in Fig. 8(a) and 8(b) the absorbance of dye solutions  
12 decreases as a function of time at pH 9 and pH 7 respectively. Fig. 8(c) for the blank solution,  
13 photocatalyst was not present in it and Fig. 8(d) and 8(e) indicates dye degradation with time and  
14 percent efficiency under different conditions, respectively. With 150 min visible light irradiation,  
15 the degradation efficiency was found 99% and 41% at pH 9 and pH 7 respectively while for the  
16 blank solution efficiency was only 6%. It was observed that the efficiency was much higher in  
17 alkaline solution (at pH 9) than neutral medium (pH 7) because of the formation of hydroxyl  
18 radicals at pH 9. In alkaline solution hydroxide ions are easily oxidized to form hydroxyl radicals  
19 which are the key fact to degrade the organic bonds of cationic dye methyl violet 6b (MV).<sup>74</sup> The  
20 inclusion of one oxide to other oxides creates defect within the crystal that lead to the formation  
21 of Schottky barrier at the interface between metal and semiconductor. As a result, hydroxyl  
22 radicals are formed that enhance the catalytic activity of mixed metal oxide nanoparticle than  
23 single metal oxide.<sup>75,76</sup>  
24  
25  
26  
27  
28  
29  
30  
31  
32  
33  
34  
35  
36  
37  
38  
39  
40  
41  
42  
43  
44  
45  
46  
47  
48  
49  
50  
51  
52  
53  
54  
55  
56  
57  
58  
59  
60

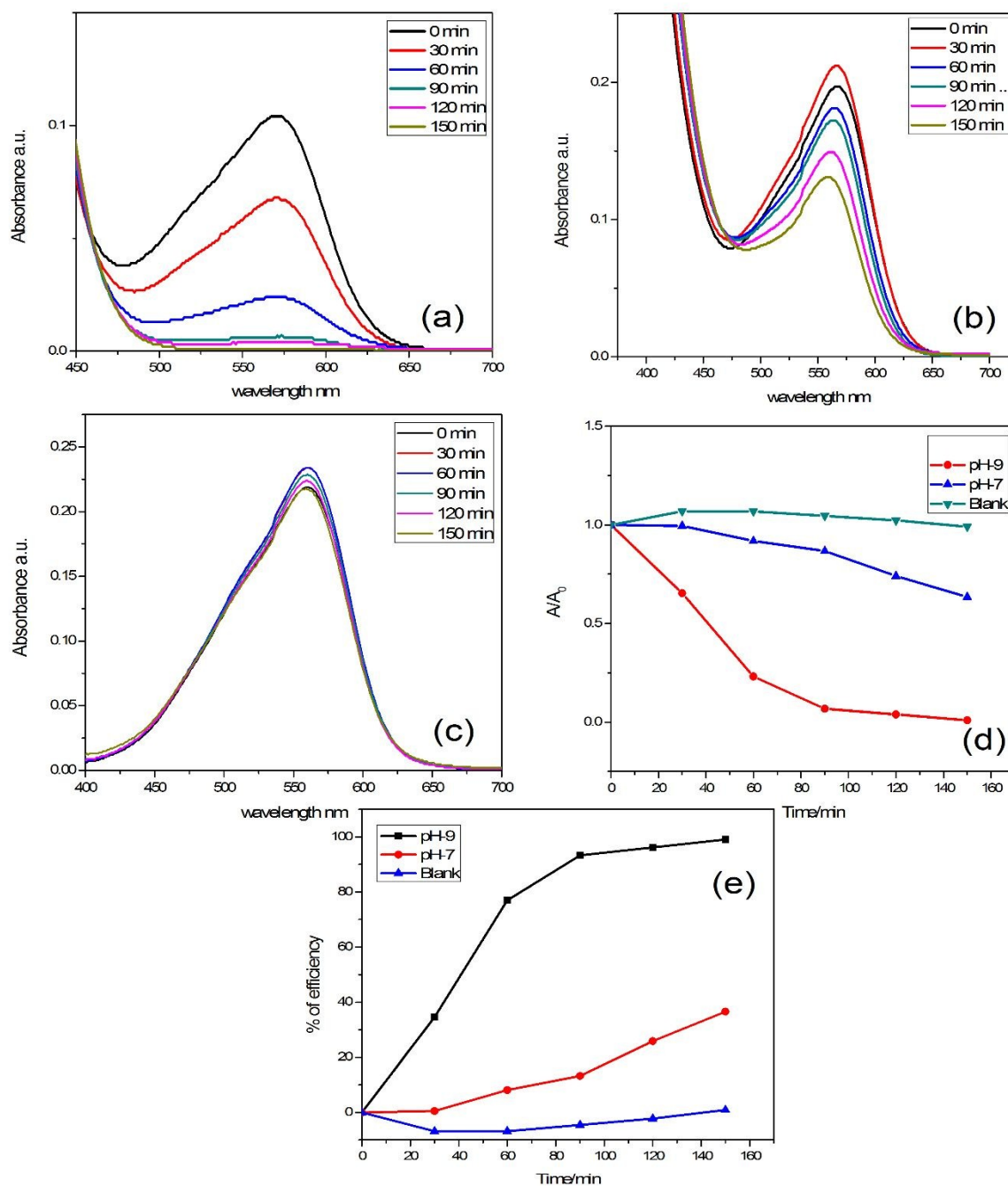


**Fig. 8** Variation of the absorption spectra of Methyl Violet 6b solution (100 ml, 50 ppm dye,  $0.05 \text{ gL}^{-1}$  dosage) under visible light irradiation at 30 min time intervals (a) catalyst at pH 9 (b) catalyst at pH 7.0; (c) blank solution (d) degradation with time and (e) indicate the percent of efficiency at pH 9, pH 7 and blank solution respectively.

### 3.11 Evaluation of catalytic stability of $\text{Ag}_2\text{O}_3 \cdot \text{SnO}_2 \cdot \text{Cr}_2\text{O}_3$ nanoparticle

The recycles and reuse of photocatalytic processes has become very exciting due to the significant contribution to lowering the operational cost of the process for waste water purification. The catalyst can be regenerated in a very simple way. The solution was kept standing for 24 h after finishing the reaction and then decanted the supernatant. By thoroughly washing the catalyst with water, it was dried at 70 °C for 2 h. Then it was reused for four times to assess the stability of photocatalyst. For each new cycle, the solution was filtered, dried and reused for the degradation of fresh MV solution under similar conditions. The results are presented in Fig. 9. The percentage of efficiency at pH 9 was 99, 90.5, 79, 74.6 and 67%. The result showed that the catalytic activity decreased consecutively as they were used for several times. This decrease in photocatalytic activity may be attributed to the structural changes of nanocomposite after several use. Furthermore, during filtration some quantity of catalyst may be lost which is another reason to decrease the photocatalytic efficiency.

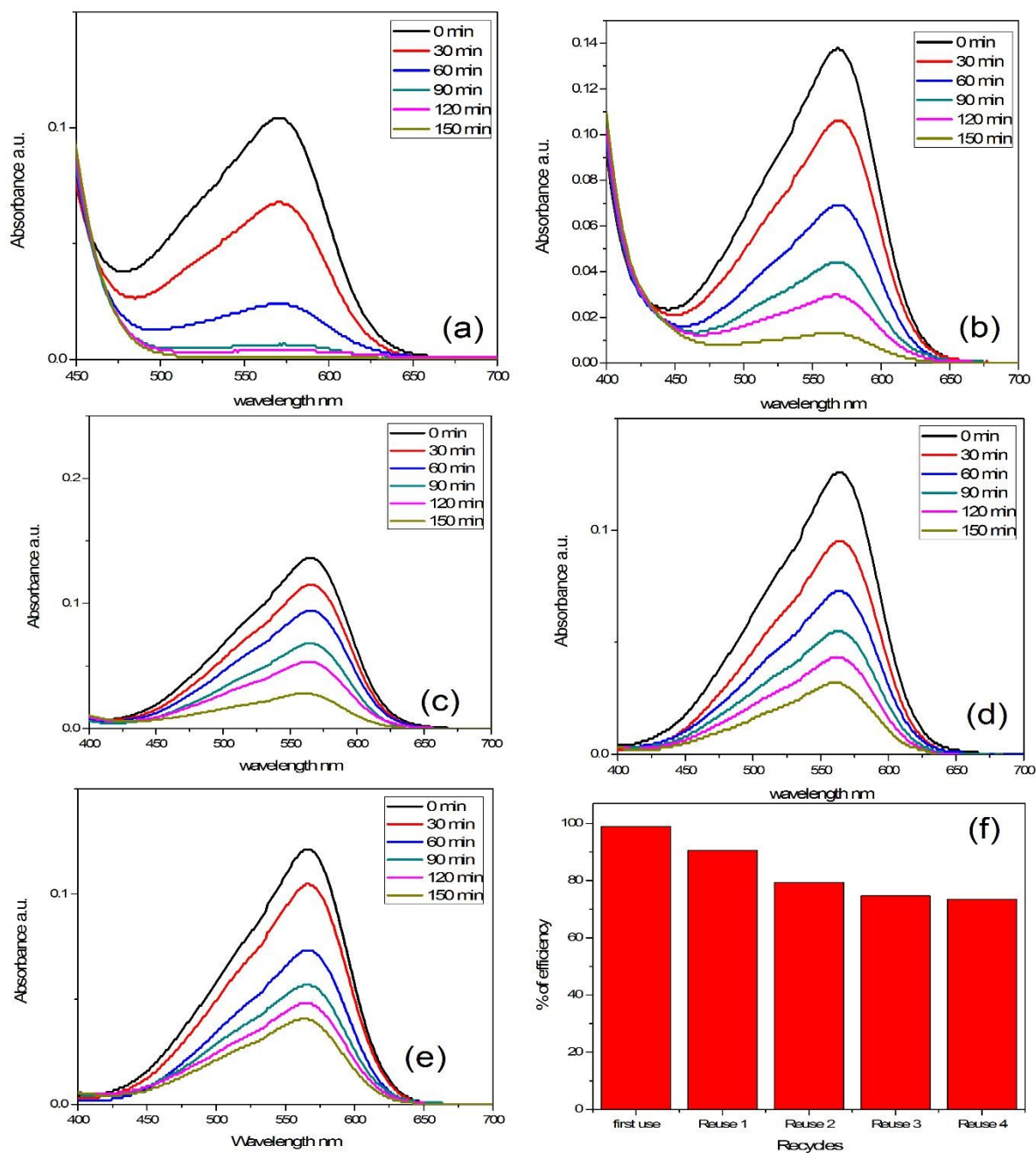


**Fig. 9** Recycle and reuse of photocatalyst for MV degradation (MV concentration: 50 ppm; photocatalyst dosage: 0.05 g L<sup>-1</sup>; irradiation time: 120 min) in the presence of the catalyst at pH 9 (a-e) decrease in absorption for 1st to 5th use and (f) % of efficiency.

### 3.12 Antibacterial test of $\text{Ag}_2\text{O}_3 \cdot \text{SnO}_2 \cdot \text{Cr}_2\text{O}_3$ nanoparticles

Nanotechnology, especially pharmaceuticals nanotechnology has attracted the attention of many researchers due to numerous advantages on the health issue.<sup>77</sup> Nowadays development of new antimicrobial therapies has become an important research topic. Nanocomposites of metal oxide and metal sulfide exhibit excellent antimicrobial property.<sup>78</sup> Having various properties, potencies, and spectra of activity some metals such as silver, copper, gold, titanium, and zinc have been used as antibacterial agent.<sup>79</sup> Antibacterial agents are also very important in the textile industry, water disinfection, medicine, and food packaging. Usually, organic compounds used for disinfection have some disadvantages, including toxicity to the human body. For this reason, the interest in inorganic disinfectants such as metal oxide nanoparticles is increasing rapidly. Inorganic nanostructured materials and their surface modifications execute good antimicrobial functions. These improved antibacterial agents in low concentrations locally destroy bacteria, without being toxic to the surrounding healthy tissues.<sup>80,81</sup> Here, the antibacterial activity of  $\text{Ag}_2\text{O}_3 \cdot \text{SnO}_2 \cdot \text{Cr}_2\text{O}_3$  nanoparticle was investigated using well diffusion method against gram-positive bacteria (*Staphylococcus aureus*) and gram-negative bacteria (*Escherichia coli*). Agar nutrients were used for the bacterial culture where the sample was introduced creating 6 mm well and Gentamicin 10 (GEN 10) was used as a reference. The different inhibition zone was measured after overnight incubation at 37 °C.<sup>82</sup> Zone of inhibition confirmed the antibacterial effect of  $\text{Ag}_2\text{O}_3 \cdot \text{SnO}_2 \cdot \text{Cr}_2\text{O}_3$  nanoparticle that killed both gram-positive and gram-negative bacteria also indicates the more effectiveness against-gram negative bacteria than gram-positive bacteria as summarized in **Table 3** and **Fig. 10**.

**Table 3** Antibacterial study of  $\text{Ag}_2\text{O}_3 \cdot \text{SnO}_2 \cdot \text{Cr}_2\text{O}_3$  nanoparticles

Bacterial culture	Diameter of inhibition zone $D_{iz}$ (mm)	Diameter of well $D_w$ (mm)	Ratio $R = D_{iz}/D_w$
<i>Staphylococcus aureus</i>	23	8	2.87
<i>Escherichia coli</i>	35	8	5.83

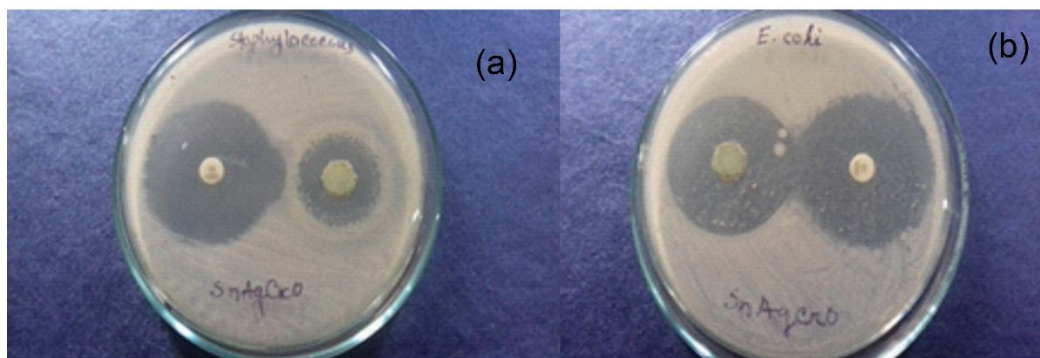


**Fig 10** Antibacterial activity of  $Ag_2O_3 \cdot SnO_2 \cdot Cr_2O_3$  nanoparticle with (a) *Staphylococcus aureus* and (b) *Escherichia coli*

### 3.13 Detection of 4-AP by $Ag_2O_3 \cdot SnO_2 \cdot Cr_2O_3$ NPs

The possible application of  $Ag_2O_3 \cdot SnO_2 \cdot Cr_2O_3$  NPs on GCE to the fabrication of an electrochemical sensor for the detection of 4-AP in phosphate buffer medium of pH 7.0 was assessed. During the fabrication process of this desire electrochemical sensor, a drop of nafion (5% nafion suspension in ethanol) was applied on modified GCE coated  $Ag_2O_3 \cdot SnO_2 \cdot Cr_2O_3$  NPs to bring the long-time stability in phosphate buffer medium. Since the nafion is a conductive copolymer, it enhanced the stability of the sensor as well as the conductance and electron transfer rate as described by the previous authors.<sup>83-88</sup> The electrochemical properties with coated and uncoated GCE electrode in 5.0 mM  $[Fe(CN)_6]^{3-/4-}$  containing 0.1 M KCl have been studied by cyclic voltammogram (CV) and EIS and included in the supporting information section (Fig. S2). The bare GC electrode gives well-defined redox peaks while NPs/GCE provides low-currents response due to the slightly blocking the electrode surface. The NPs/GCE exhibited

substantial redox currents in comparison with those exhibited by the GCE electrode, which demonstrated the most auspicious catalytic performance in presence of 4-AP. The EIS spectra (5.0 mM  $[\text{Fe}(\text{CN})_6]^{3-/4-}$  containing 0.1 M KCl) were recorded to explore the relative charge transfer of the modified electrodes with NPs coated and uncoated GCE as shown in Fig. S2b. Control experiment of 4-AP response with the fabrication of various mono and binary metal oxides onto GCE were performed and presented in Fig. S3. In Fig. S3a, the sensor performance of three  $\text{Ag}_2\text{O}_3/\text{GCE}$ ,  $\text{SnO}_2/\text{GCE}$ ,  $\text{Cr}_2\text{O}_3/\text{GCE}$  electrodes for the detection of 4-AP was compared with ternary  $\text{Ag}_2\text{O}_3 \cdot \text{SnO}_2 \cdot \text{Cr}_2\text{O}_3$  NPs/GCE electrode. Here, the highest response was observed for the detection of 4-AP with the ternary  $\text{Ag}_2\text{O}_3 \cdot \text{SnO}_2 \cdot \text{Cr}_2\text{O}_3$  NPs/GCE electrode compared with single metal oxides. Binary metal oxide performances were also analyzed and compared with  $\text{Ag}_2\text{O}_3 \cdot \text{SnO}_2 \cdot \text{Cr}_2\text{O}_3$  NPs/GCE fabricated electrode in identical conditions and presented in Fig. S3b. In this case too, the highest response was observed for the detection of 4-AP with the ternary  $\text{Ag}_2\text{O}_3 \cdot \text{SnO}_2 \cdot \text{Cr}_2\text{O}_3$  NPs/GCE electrode compared with binary metal oxide. These control experiments clearly indicated the enhanced 4-AP sensor performance of the trimetallic  $\text{Ag}_2\text{O}_3 \cdot \text{SnO}_2 \cdot \text{Cr}_2\text{O}_3$  nanocomposite.

The electrochemical response is measured on the surface of the thin film of  $\text{Ag}_2\text{O}_3 \cdot \text{SnO}_2 \cdot \text{Cr}_2\text{O}_3$  NPs/binder/GCE. The holding period in the electrometer is set as 1.0 sec. At the very beginning of this study, the numerous environmental toxins were analyzed using the recently assembled electrochemical sensor based on  $\text{Ag}_2\text{O}_3 \cdot \text{SnO}_2 \cdot \text{Cr}_2\text{O}_3$  NPs/binder/GCE sensor and this performance was executed at potential 0~+1.5V and 0.1  $\mu\text{M}$  of each toxin in phosphate buffer medium of pH 7.0. The Fig. 11(a) represents the electrochemical responses of 2-AP, 3-MP, 4-AP, 4-hexylresorcinol, melamine, M-THydhCl, PHydh, zimaldehyd and obviously, 4-AP shows the highest current response comparing to other toxins. Therefore, on the basis of the

1  
2  
3 supreme I-V response, 4-AP is identified as a selective toxin to the sensor assembly. To examine  
4 the I-V responses of 4-AP in the various buffer medium with distinguished pH value, a test was  
5 performed as illustrated in Fig. 11(b). From the observation in Fig. 11(b), 4-AP is found to show  
6 the maximum electrochemical activity in the phosphate buffer medium of pH 7.0. After that, 4-  
7 AP was subjected to analyze with distinct concentration ranging in a sequence from  
8 0.1mM~0.1nM and the resulted I-V responses are explored in Fig. 11(c). As it is demonstrated in  
9 Fig. 11(c), the electrochemical responses can be distinguished from lower to a higher  
10 concentration of 4-AP. This similar characteristic of the electrochemical sensor has reported to  
11 the detection of the various toxins in our previous articles<sup>89-92</sup> and it provides evidence that the I-  
12 V responses are varied directly with the corresponding concentration of 4-AP. To establish the  
13 calibration of the proposed 4-AP chemical sensor, the current data are separated from Fig. 11(c)  
14 at potential +1.5V and plotted as current vs. concentration as illustrated in Fig. 11(d), which is  
15 defined as a calibration curve. As it is seeming from Fig. 11(d), the current data are linearly  
16 distributed with corresponding concentration from 0.1nM to 0.01mM known as linear dynamic  
17 range (LDR). Perceptibly, the resultant LRD is very a wider range of concentration. The  
18 sensitivity of the proposed 4-AP chemical sensor is equal to  $25.1962 \mu\text{A}\mu\text{M}^{-1}\text{cm}^{-2}$  and it is  
19 calculated from the slope of the calibration curve ( $0.7962 \mu\text{A}\mu\text{M}^{-1}$ ) and cross-sectional area of  
20 GCE ( $0.0316 \text{ cm}^2$ ). Perceivably, the obtained sensitivity is appreciable. Applying the signal to  
21 noise ratio of 3, the detection limit (DL) is estimated and an appreciable result around  
22  $98.41 \pm 4.92 \text{ pM}$  is experimented. To determine the linearity of LDR, log (conc.) vs current is  
23 plotted as in Fig. 11(d) inset and as it is illustrated, the current data are fitted with the regression  
24 co-efficient  $R^2=0.9986$ , provides the evidence of linearity of LDR.  
25  
26  
27  
28  
29  
30  
31  
32  
33  
34  
35  
36  
37  
38  
39  
40  
41  
42  
43  
44  
45  
46  
47  
48  
49  
50  
51  
52  
53  
54  
55  
56  
57  
58  
59  
60

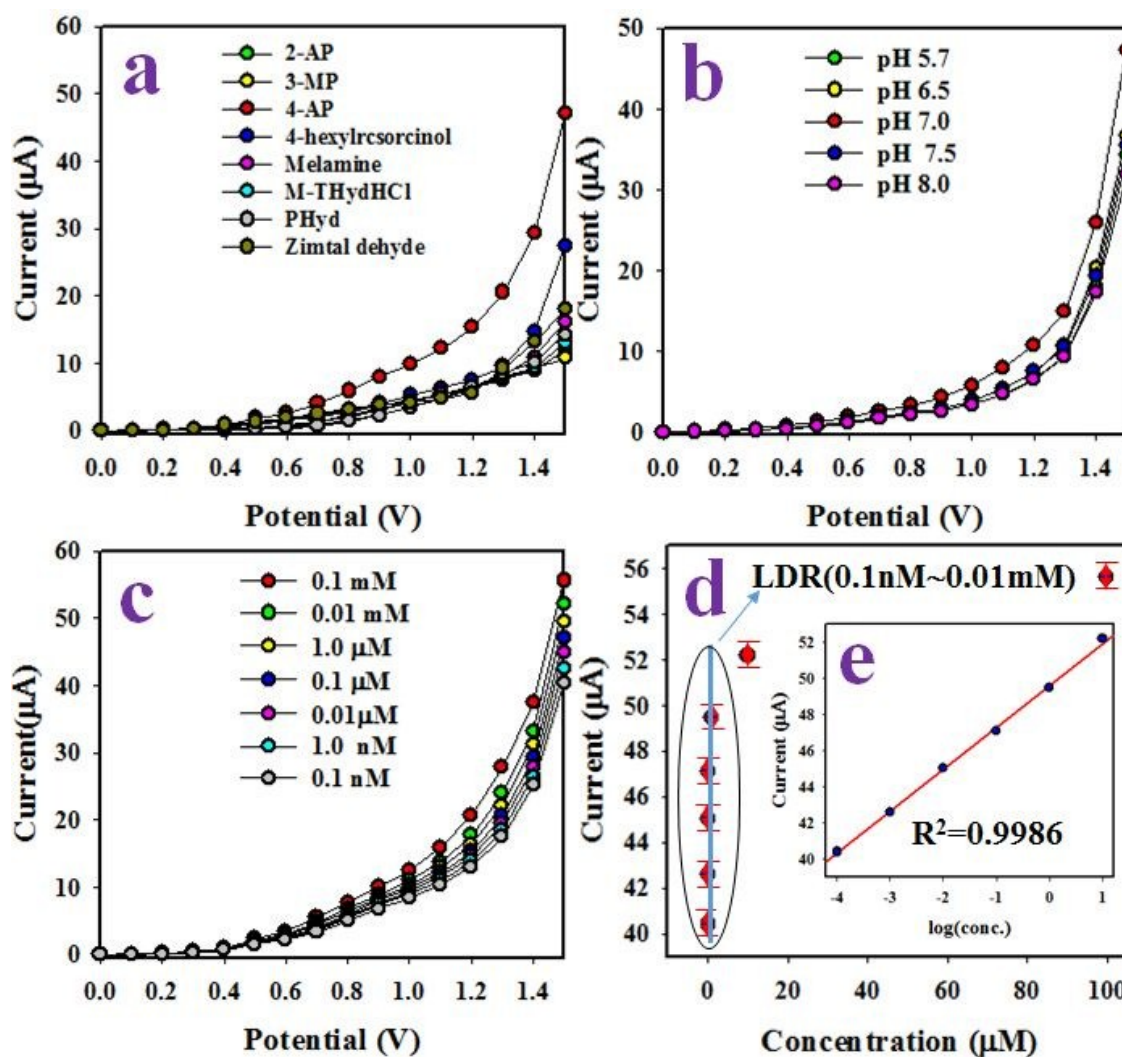


**Fig. 11** Optimization of sensor analytical performances of  $\text{Ag}_2\text{O}_3 \cdot \text{SnO}_2 \cdot \text{Cr}_2\text{O}_3$  NPs/binder/GCE electrode, (a) selectivity assessment with analytes concentration  $0.1 \mu\text{M}$ , (b) pH optimization at  $0.1 \mu\text{M}$  4-AP, (c) electrochemical (I-V) responses to 4-AP concentration, and (d) exploration of calibration curve [inset:  $\log(4\text{-AP-conc.})$  vs current].

The ability to perform similar electrochemical response in identical conditions is very important measurable analytical performance of an electrochemical sensor. Thus, this test was executed using  $0.1 \mu\text{M}$  concentration of 4-AP and potential 0 to +1.5V as illustrated in Fig. 12(a).

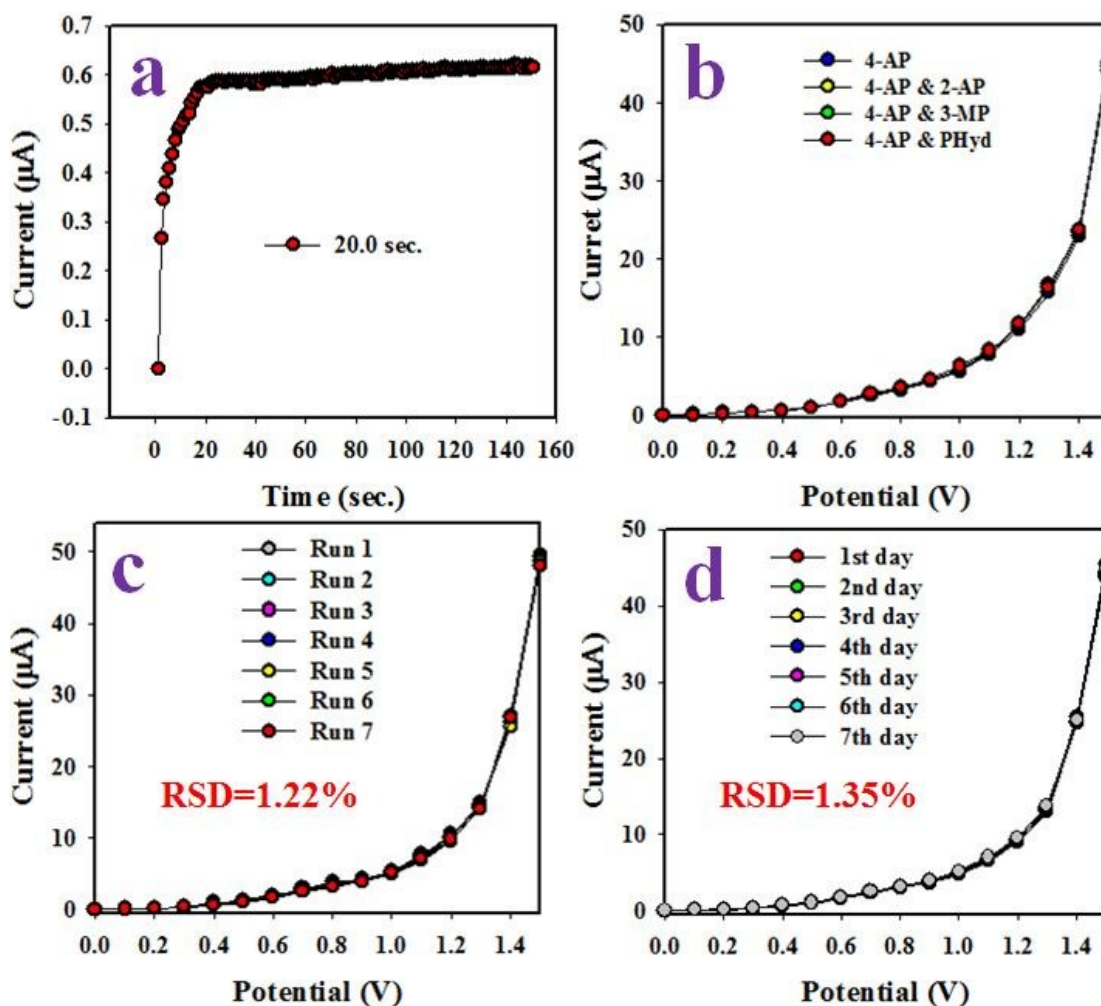


**Fig. 12** Evaluation of reliability performance of 4-AP sensor with  $\text{Ag}_2\text{O}_3 \cdot \text{SnO}_2 \cdot \text{Cr}_2\text{O}_3$  NPs/binder/GCE. (a) Response time for 4-AP with concentration  $0.1 \mu\text{M}$ , (b) the interference test of 4-AP sensor with analytes concentration of  $0.1 \mu\text{M}$  at pH 7.0, (c) the reproducibility test with 4-AP concentration of  $0.1 \mu\text{M}$  and (d) the longtime performance test of 4-AP sensor.

The response is defined as the time required to complete an electrochemical analysis and it is an efficiency measurement criterion. Therefore, the 4-AP sensor based on  $\text{Ag}_2\text{O}_3 \cdot \text{SnO}_2 \cdot \text{Cr}_2\text{O}_3$  NPs/binder/GCE was subjected to measure the response time and it was experimented with  $0.1 \mu\text{M}$  of 4-AP in phosphate buffer medium with pH 7.0 as illustrated in Fig. 12(a). From Fig. 12(a), it is shown that 4-AP sensor is able to produce a steady state I-V response within 20.0 sec and the obtained result is highly appreciable. As it is demonstrated in Fig. 12(b), the I-V responses of 4-AP do not deviate from its original value in the presence of

other analytes such as 2-AP, 3-MP, and Phyd with 0.1  $\mu\text{M}$  concentration at potential ranging as 0~+1.5V in phosphate buffer medium. Therefore, it provides evidence that the 4-AP sensor is highly selective toward the 4-AP analyte only. The reproducibility of an electrochemical sensor is the most important analytical performance and it is the symbol of the reliability of the sensor. As it is perceived from Fig. 12(c), the electrochemical responses are replicated and completely impossible to distinguish and it is not changed even washing of electrode after each run. Thus, it provides information about the reliability of this method and it is able to analyze the real samples. This test was experimented using 0.1  $\mu\text{M}$  4-AP at applied potential 0~+1.5V in buffer medium with pH 7.0. The precision of I-V response for reproducibility performance at potential +1.5 was calculated and it is found to be 1.22% in-term of relative standard deviation (RSD). Thus, it confirmed the high precision of the reproducibility test. This similar test was executed at similar identical conditions to evaluate the information about the stability of 4-AP chemical sensor based on  $\text{Ag}_2\text{O}_3 \cdot \text{SnO}_2 \cdot \text{Cr}_2\text{O}_3$  NPs/binder/GCE in phosphate buffer medium as presented in Fig. 12(d). From Fig. 12(d), the analogous observation like reproducibility in Fig. 12(c) is observed during a long duration of around seven days. Therefore, the proposed 4-AP chemical sensor has the stability to perform in an elongated period, in a phosphate buffer medium. To find out the validity of this study, a comparison between the similar research works is presented in

**Table 4** as following in term of sensitivity, LDR and DL.<sup>93-95</sup>

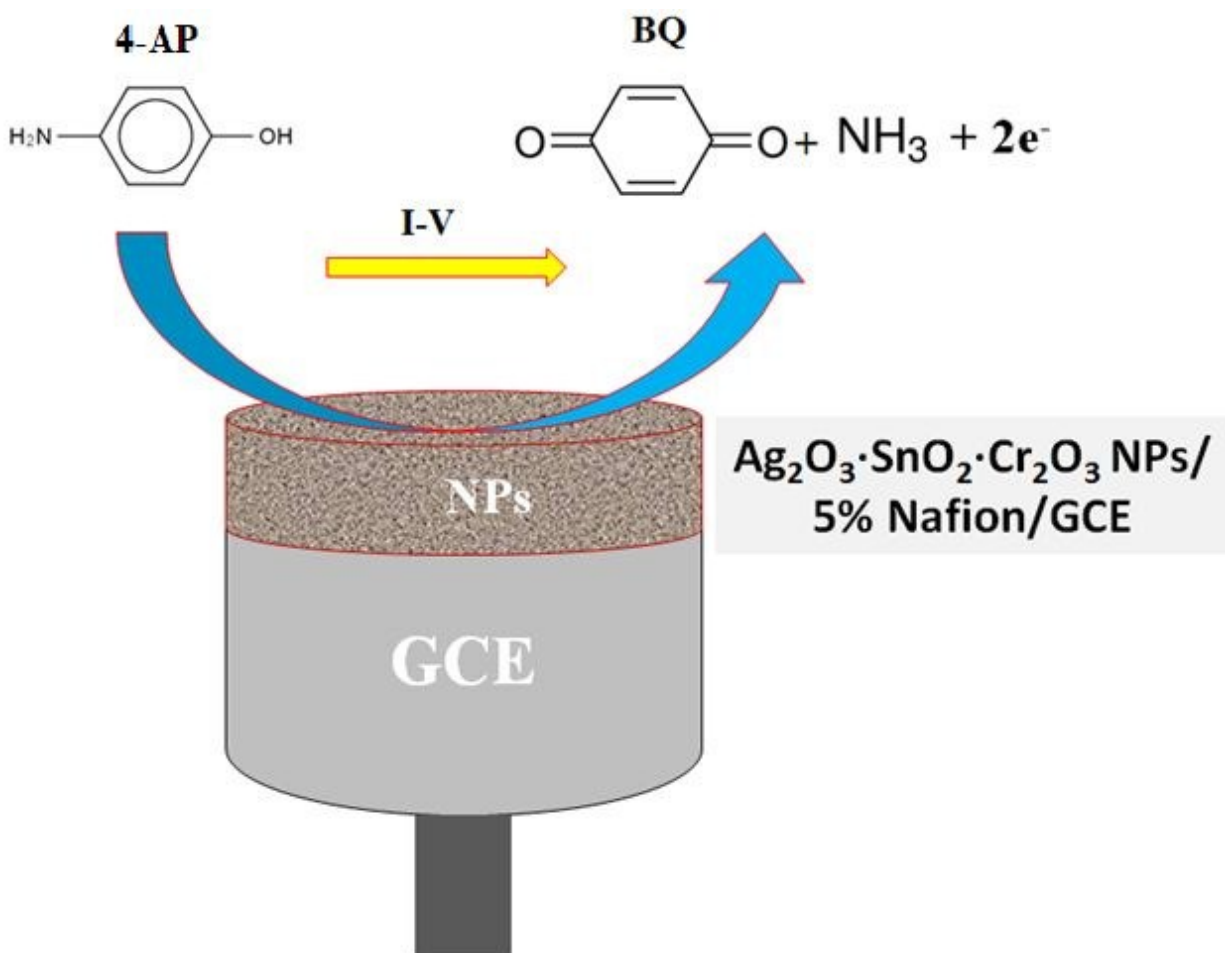
**Table 4.** Comparison of analytical performances with  $\text{Ag}_2\text{O}_3 \cdot \text{SnO}_2 \cdot \text{Cr}_2\text{O}_3$  NPs/binder/GCE for 4-AP sensors.

Modified GCE	DL	LDR	Sensitivity	Ref.
$\text{Ag}_2\text{O}/\text{CuO}$ NSs/GCE	3.31 pM	0.1 nM~ 0.1mM	0.028 mA $\mu\text{M}^{-1}\text{cm}^{-2}$	[93]
$\text{ZnO}/\text{Yb}_2\text{O}_3$ NSs/GCE	19.0 pM	0.1 nM~0.1 mM	5.063 $\mu\text{A} \mu\text{M}^{-1}\text{cm}^{-2}$	[94]
PANI/G/CNTs NCs/GCE	63.4 pM	0.1 nM~ 0.01 M	2.187 $\mu\text{A} \mu\text{M}^{-1}\text{cm}^{-2}$	[95]
$\text{Ag}_2\text{O}_3 \cdot \text{SnO}_2 \cdot \text{Cr}_2\text{O}_3$ NPs/GCE	98.41 pM	0.1 nM~0.01mM	25.19 $\mu\text{A} \mu\text{M}^{-1}\text{cm}^{-2}$	This study

\*DL (detection limit), LDR (linear dynamic range), pM(picomole), mM(millimole).

1  
2  
3  
4  
5 The electrochemical oxidation of 4-AP on Ag<sub>2</sub>O<sub>3</sub>·SnO<sub>2</sub>·Cr<sub>2</sub>O<sub>3</sub> NPs/binder/GCE sensor is  
6 illustrated in **Scheme 1**. During electrochemical analysis, the 4-AP is absorbed on the surface of  
7 Ag<sub>2</sub>O<sub>3</sub>·SnO<sub>2</sub>·Cr<sub>2</sub>O<sub>3</sub> NPs/binder/GCE and oxidize to benzoquinone and ammonia at applied  
8 potential 0 to +1.5V. At the time of oxidation of 4-AP, a number of electrons are generated in the  
9 phosphate buffer medium and enhanced the conductivity is observed in the sensing medium. As  
10 a result, the amplification in electrochemical responses is perceived as previous reports.<sup>93,96</sup> The  
11 mechanism of electrochemical oxidation in applied potential is illustrated in **Scheme 1** and the  
12 corresponding reaction (i) is supposed as





**Scheme 1.** The electrochemical oxidation of 4-AP based on Ag<sub>2</sub>O<sub>3</sub>·SnO<sub>2</sub>·Cr<sub>2</sub>O<sub>3</sub> NPs/binder/GCE sensor.

Shortly, it can be noticed that the projected 4-AP electrochemical sensor based on Ag<sub>2</sub>O<sub>3</sub>·SnO<sub>2</sub>·Cr<sub>2</sub>O<sub>3</sub> NPs/binder/GCE exhibits good performances in term of sensitivity, linear dynamic range, detection limit, reproducibility, stability and response time.

### 3.14 Investigation of real samples

Finally, the fabricated 4-AP chemical sensor based on Ag<sub>2</sub>O<sub>3</sub>·SnO<sub>2</sub>·Cr<sub>2</sub>O<sub>3</sub> NPs binder/GCE was applied to detect 4-AP in real environmental samples using the recovery method. The real environmental samples are collected from industrial effluents, extracted from a

PVC water bottle and food packaging bags. The resulted data are presented in **Table 5** and it is appeared to be quite satisfactory.

**Table 5.** The analysis of real environmental samples using  $\text{Ag}_2\text{O}_3 \cdot \text{SnO}_2 \cdot \text{Cr}_2\text{O}_3$  NPs/GCE chemical sensor by recovery method.

Sample	Added 4-AP concentration ( $\mu\text{M}$ )	Measured 4-AP conc. <sup>a</sup> by $\text{Ag}_2\text{O}_3 \cdot \text{SnO}_2 \cdot \text{Cr}_2\text{O}_3$ NPs/binder/GCE ( $\mu\text{M}$ )			Average recovery <sup>b</sup> (%)	RSD <sup>c</sup> (%) (n=3)
		R1	R2	R3		
Industrial effluent	0.0100	0.00981	0.00962	0.00975	97.27	1.00
PC- water bottle	0.01000	0.00945	0.00974	0.00957	95.87	1.52
PVC- food packaging bag	0.01000	0.01123	0.01096	0.01085	110.13	1.78

<sup>a</sup>Mean of three repeated determination (signal to noise ratio 3)  $\text{Ag}_2\text{O}_3 \cdot \text{SnO}_2 \cdot \text{Cr}_2\text{O}_3$  NPs/binder/GCE.

<sup>b</sup>Concentration of 4-AP determined/Concentration taken. (Unit: nM)

<sup>c</sup>Relative standard deviation value indicates precision among three repeated measurements (R1, R2, R3).

#### 4. Conclusions

In summary, an easy synthetic method has been used for the synthesis of  $\text{Ag}_2\text{O}_3 \cdot \text{SnO}_2 \cdot \text{Cr}_2\text{O}_3$  NP and its application as an efficient photocatalyst. This inexpensive, facile and easily controllable synthetic method can improve physicochemical interaction between the nano-particulate and active material sites. The synthesized nanoparticle is characterized by XRD, SEM, EDS with mapping, XPS, UV-Visible, Photoluminescence, Zetasizer, and FTIR Spectroscopy. From XRD, the particle size was calculated as 34.6 nm. The band-gap was found to be 3.06 eV from UV-Visible measurement. This nanoparticle exhibits excellent efficiency in dye degradation. It has 99% degradation efficiency under visible light in pH 9 within 150 minutes. The small size, negative zeta potential, suitable band-gap and different morphologies of the component oxides might be responsible for the high photocatalytic efficiency. Calcination temperature-dependent PL properties were observed. The nanoparticle also showed affinity to

1  
2  
3 attack both gram-positive and gram-negative bacteria. The fabricated electrochemical sensor  
4 with  $\text{Ag}_2\text{O}_3 \cdot \text{SnO}_2 \cdot \text{Cr}_2\text{O}_3$  NPs/binder/GCE was also used to detect 4-AP in a phosphate buffer  
5 medium at room conditions. The sensor analytical performances including sensitivity  
6 (25.1962  $\mu\text{A} \mu\text{M}^{-1} \text{cm}^{-2}$ ), LDR (0.1nM~0.01mM), DL (98.41±4.92pM), reproducibility, and  
7 response time were measured by electrochemical method. The sensor probe fabricated as  
8  $\text{Ag}_2\text{O}_3 \cdot \text{SnO}_2 \cdot \text{Cr}_2\text{O}_3$  NPs/binder/GCE was also validated to detect in real environmental samples  
9 and found satisfactory results.

### 10 Acknowledgments

11 Fulbright USA is gratefully acknowledged by Dr. Md Abdus Subhan for awarding  
12 Fulbright Visiting Scholar Award 2018-2019. Center of Excellence for Advanced Materials  
13 Research (CEAMR), Chemistry Department, King Abdulaziz University, Jeddah, Saudi Arabia  
14 is highly acknowledged for financial support and research facilities.

### 15 References

- 16 1. S. V. Merzlikin, N. N. Tolkachev, L. E. Briand, T. Strunskus, C. Wöll, I. E. Wachs and  
17 W. Grünert, *Angew. Chem., Int. Ed.*, 2010, 49, 8037-8041.
- 18 2. J. Geserick, T. Fröschl, N. Hüsing, G. Kucerova, M. Makosch, T. Diemant and R. J.  
19 Behm, *Dalton Trans.*, 2011, 40, 3269-3286.
- 20 3. S. M. Saqer, D. I. Kondarides and X. E. Verykios, *Appl. Catal., B*, 2011, 103, 275-286.
- 21 4. J. A. Rodriguez and D. Stacchiola, *Phys. Chem. Chem. Phys.*, 2010, 12, 9557-9565.
- 22 5. J. B. Park, J. Graciani, J. Evans, D. Stacchiola, S. Ma, P. Liu and J. A. Rodriguez, *Proc.*  
23 *Natl. Acad. Sci.*, 2009, 0812604106.
- 24 6. L. I. Nadaf and K. S. Venkatesh, *J. Appl. Chem.*, 2016, 9, 1-4.

7. J. A. Rodriguez, X. Wang, J. C. Hanson, G. Liu, A. Iglesias-Juez and M. Fernández-García, *J. Chem. Phys.* 2003, 119, 5659-5669.
8. H. Cui, M. Zayat and D. Levy, *J. Sol-Gel Sci. Technol.*, 2005, 35, 175-181.
9. Y. J. Kim, S. B. Rawal, S. D. Sung and W. I. Lee, *Bull. Korean Chem. Soc.*, 2011, 32, 141-144.
10. B. M. Reddy, B. Chowdhury and P. G. Smirniotis, *Appl. Catal., A*, 211(1), 19-30.
11. V. V. Zyryanov, *Inorg. Mater.*, 2003, 39, 1163-1171.
12. S. Ajaikumar and A. Pandurangan, *Appl. Catal., A*, 2009, 357, 184-192.
13. W. C. Sheets, E. S. Stamper, H. Kabbour, M. I. Bertoni, L. Cario, T. O. Mason and K. R. Poeppelmeier, *Inorg. Chem.*, 2007, 46, 10741-10748.
14. D. Jiang, L. Su, L. Ma, N. Yao, X. Xu, H. Tang and X. Li, *Appl. Surf. Sci.*, 2010, 256, 3216-3223.
15. B. M. Reddy, I. Ganesh, E. P. Reddy, A. Fernández and P. G. Smirniotis, *Russ. J. Phys. Chem. B*, 2001, 105, 6227-6235.
16. C. Pascal, J. L. Pascal, F. Favier, M. L. E. Moubtassim and C. Payen, *Chem. Mater.*, 1999, 11, 141-147.
17. B. Martinez, A. Roig, E. Molins, T. Gonzalez-Carreno and C. J. Serna, *J. Appl. Phys.*, 1998, 83, 3256-3262.
18. M. D. P. Morales, S. Veintemillas-Verdaguer, M. I. Montero, C. J. Serna, A. Roig, L. Casas and F. Sandiumenge, *Chem. Mater.*, 1999, 11, 3058-3064.
19. C. Branci, N. Benjelloun, J. Sarradin and M. Ribes, *Solid State Ionics*, 2000, 135, 169-174.
20. Z. R. Hong, C. J. Liang, X. Y. Sun and X. T. Zeng, *J. Appl. Phys.*, 2006, 100, 093711.
21. P. C. Pandey, B. C. Upadhyay, C. M. D. Pandey and H. C. Pathak, *Sens. Actuators, B*, 1999, 56, 112-120.
22. G. C. Bond, L. R. Molloy and M. J. Fuller, *Journal of the Chemical Society, Chem. Commun.*, 1975, 19, 796-797.
23. Y. S. Cho, G. R. Yi, J. J. Hong, S. H. Jang and S. M. Yang, *Thin Solid Films*, 2006, 515, 1864-1871.
24. M. M. Rahman, M. M. Alam, A. M. Asiri and M. A. Islam, *Talanta*, 2017, 170, 215-223.
25. M. M. Rahman, M. M. Alam and A. M. Asiri, *New J. Chem.*, 2017, 41, 9938-9946

- 1  
2  
3  
4  
5  
6  
7  
8  
9  
10  
11  
12  
13  
14  
15  
16  
17  
18  
19  
20  
21  
22  
23  
24  
25  
26  
27  
28  
29  
30  
31  
32  
33  
34  
35  
36  
37  
38  
39  
40  
41  
42  
43  
44  
45  
46  
47  
48  
49  
50  
51  
52  
53  
54  
55  
56  
57  
58  
59  
60
26. M. A. Subhan, P. C. Saha, S. A. Sumon, J. Ahmed, A. M. Asiri, M. M. Rahman and M. Al-Mamun, *RSC Adv.*, 2018, 8, 33048–33058.
27. A. Verma and M. S. Mehata, *J. Radiat. Res. Appl. Sci.*, 2016, 9, 109–115.
28. X. Yang, X. Peng, C. Xu and F. Wang, *J. Electrochem. Soc.*, 2009, 156, C167-C175.
29. C. L. Li, H. X. Zhao, T. Takahashi, and M. Matsumura, *Mater. Sci. Eng., A*, 2001, 308, 268-276.
30. J. Y. Hwang and D. S. Seo, *J. Electrochem. Soc.*, 2010, 157, J351-J357.
31. M. Freemantle, *Chemical and Engineering News Archive*, 1998, 76, 8.
32. J. I. Fasick, N. Lee and D. D. Oprian, Spectral tuning in the human blue cone pigment. *Biochemistry*, 1999, 38, 11593-11596.
33. H. Rotter, M.V. Landau, M. Carrera, D. Goldfarb and M. Herskowitz, *Appl. Catal., B*, 2004, 47, 111-126.
34. H. Rotter, M. V. Landau and M. Herskowitz, *Environ. Sci. Technol.*, 2005, 39, 6845-6850.
35. M.M. Rahman, S.B. Khan, H.M. Marwani, A.M. Asiri, K.A. Alamry, M.A. Rub, A. Khan, A.A.P. Khan, A.H. Qusti. *J. Indust. Engineering Chem.* 2014, 20, 1071-1078.
36. A. Khan, A.A.P. Khan, A.M. Asiri, M.A. Rub, M.M. Rahman, S.A. Ghani. *Microchim. Acta* 2014, 181, 1049-1057.
37. M.M. Rahman, S.B. Khan, H.M. Marwani, A.M. Asiri. *J. Taiwan Institute of Chem. Engineers.* 2014, 45, 1964-1974.
38. M.M. Alam, A.M. Asiri, M.T. Uddin, M. A. Islam and M. M. Rahman, *ChemistrySelect*, 2018, 3, 11460–11468.
39. M. M. Alam, A. M. Asiri, M. T. Uddin, M. A. Islam and M. M. Rahman, *RSC Adv.*, 2018, 8, 12562–12572.
40. J. P. Cheng, X. B. Zhang, X. Y. Tao, H. M. Lu, Z. Q. Luo and F. Liu, *J. Phys. Chem. B*, 2006, 110, 10348-10353.
41. I. M. Banat, P. Nigam, D. Singh and R. Marchant, *Bioresour. Technol.*, 1996, 58, 217-227.
42. M. E. Bosch, A. R. Sánchez, F. S. Rojas and C. B. Ojeda, *J. Pharm. Biomed. Anal.*, 2006, 42, 291-321.
43. F. L. Martin and A. E. McLean, *Drug Chem. Toxicol.*, 1998, 21, 477-494.

- 1  
2  
3  
4  
5  
6  
7  
8  
9  
10  
11  
12  
13  
14  
15  
16  
17  
18  
19  
20  
21  
22  
23  
24  
25  
26  
27  
28  
29  
30  
31  
32  
33  
34  
35  
36  
37  
38  
39  
40  
41  
42  
43  
44  
45  
46  
47  
48  
49  
50  
51  
52  
53  
54  
55  
56  
57  
58  
59  
60
44. C. A. Mugford, and J. B. Tarloff, *Toxicology letters*, 1997, 93, 15-22.
45. K. Vijayakaran, K. Kannan, M. Kesavan, S. Suresh, P. Sankar, S. K. Tandan and S. N. Sarkar, *Environ. Toxicol. Pharmacol.*, 2014, 37, 438-447.
46. The European Pharmacopeial Convention, *The European Pharmacopeial Convention*, 2007, 49
47. The United States Pharmacopeial Convention, *The United States Pharmacopeial Convention*, 2004, 2494.
48. H. Yin, Q. Ma, Y. Zhou, S. Ai and L. Zhu, *Electrochim. Acta*, 2010, 55, 7102-7108.
49. Q. Chu, L. Jiang, X. Tian and J. Ye, *Anal. Chim. Acta*, 2008, 606, 246-251.
50. T. Pérez-Ruiz, C. Martínez-Lozano, V. Tomás and R. Galera, *J. Pharm. Biomed. Anal.*, 2005, 38, 87-93.
51. B. C. Lourenção, R. A. Medeiros, R. C. Rocha-Filho, L. H. Mazo and O. Fatibello-Filho, *Talanta*, 2009, 78, 748-752.
52. A. Brega, P. Prandini, C. Amaglio and E. Pafumi, *J. Chromatogr. A*, 1990, 535, 311-316.
53. C. M. Zou, H. Yu and M. Y. Wang, *Chin. Chem. Lett.*, 2014, 25, 201-204.
54. B. Schultz, *J. Chromatogr. A*, 1984, 299, 484-486.
55. M. S. Bloomfield, *Talanta*, 2002, 58, 1301-1310.
56. A. B. Vishnikin, M. K. Al-Shwaiyat, G. A. Petrushina, L. P. Tsiganok, V. Andruch, Y. R. Bazel and P. Solich, *Talanta*, 2012, 96, 230-235.
57. X. Zhuang, D. Chen, S. Zhang, F. Luan and L. Chen, *Microchim. Acta*, 2018, 185, 166.
58. D. Chen, X. Zhuang, J. Zhai, Y. Zheng, H. Lu and L. Chen, *Sens. Actuators, B*, 2018, 255, 1500–1506.
59. X. Zhuang, D. Chen, S. Wang, H. Liu and L. Chen, *Sens. Actuators, B*, 2017, 251, 185–191.
60. F. Luan, S. Zhang, D. Chen, K. Zheng and X. Zhuang, *Talanta*, 2018, 182, 529–535.
61. Y. Dong, M. Zhou and L. Zhang, *Electrochim. Acta*, 2019, 302, 56-64.
62. M.M. Rahman, S.B. Khan, H.M. Marwani, A.M. Asiri. *Microchimica Acta* 2015, 182, 579-588.
63. M.M. Rahman, A.M. Asiri. *Biomedical Microdevices*. 2015, 17, 1-9.
64. M.M. Rahman, A.M. Asiri. *Sensors & Actuators B: Chemical*. 2015, 214, 82-91.

- 1  
2  
3  
4  
5  
6  
7  
8  
9  
10  
11  
12  
13  
14  
15  
16  
17  
18  
19  
20  
21  
22  
23  
24  
25  
26  
27  
28  
29  
30  
31  
32  
33  
34  
35  
36  
37  
38  
39  
40  
41  
42  
43  
44  
45  
46  
47  
48  
49  
50  
51  
52  
53  
54  
55  
56  
57  
58  
59  
60
65. M.A. Hasnat, J.A. Safwan, M.S. Islam, Z. Rahman, M.R. Karim, T.J. Pirzada, A.J. Samed, M.M. Rahman. *J. Indust. Engineering Chem.* 2015, 21, 787–791.
66. S.A. El-Daly, M.M. Rahman, K.A. Alamry, A.M. Asiri. *J. Luminescence.* 2014, 148, 303-306.
67. M. Hasnat; S.B. Aoun; S.M.N. Uddin; M.M. Alam, P.P. Koay, S. Amertharaj, M.A. Rashed, M.M. Rahman, N. Mohamed. *Applied Catalysis A: General* 2014, 478, 259-266.
68. M. Faisal, S.B. Khan, M.M. Rahman, A.A. Ismail. *J. Taiwan Institute of Chem. Engineers.* 2014, 45, 2733-2741.
69. S.B. Khan, M.M. Rahman, H.M. Marwani, A.M. Asiri, K.A. Alamry. *J. Taiwan Institute of Chem. Engineers.* 2014, 45, 2770-2776.
70. M.M. Rahman, S.B. Khan, H.M. Marwani, A.M. Asiri. *PLoS ONE* 2014, 9, e114084.
71. S.B. Khan, M.M. Rahman, K. Akhtar, A.M. Asiri. *PLOS ONE* 2014, 9, e109423.
72. S. Maensiri, C. Masingboon, P. Laokul, W. Jareonboon, V. Promarak, P. L. Anderson and S. Seraphin, *Cryst. Growth Des.*, 2007, 7, 950-955.
73. S. Gnanam and V. Rajendran, *J. Sol-Gel Sci. Technol.*, 2011, 58, 62-69.
74. J. Nishio, M. Tokumura, H. T. Znad and Y. Kawase, *J. Hazard. Mater.*, 2006, 138, 106-115.
75. N. Morales-Flores, U. Pal and E. S. Mora, *Appl. Catal., A*, 2011, 394, 269-275.
76. Z. M. Yang, P. Zhang, Y. H. Ding, Y. Jiang, Z .L. Long and W. L. Dai, *Mater. Res. Bull.* 2011, 46, 1620–1628.
77. K. Adibkia, Y. Omid, M. R. Siahi, A. R. Javadzadeh, M. Barzegar-Jalali, J. Barar and A. Nokhodchi, *J. Ocul. Pharmacol. Ther.*, 2007, 23, 421-432.
78. J. L. Hu, Q. H. Yang, H. Lin, Y. P. Ye, Q. He, J. N. Zhang and H. S. Qian, *Nanoscale*, 2013, 5, 6327-6332.
79. C. Malarkodi, S. Rajeshkumar, K. Paulkumar, M. Vanaja, G. Gnanajobitha and G. Annadurai, *Bioinorg. Chem. Appl.*, 2014, 347167.
80. J. H. Mohammad, M. F. Katharina, A. A. Ali, J. A. Dorleta, R. L. Idoia, R. Teofilo, S. Vahid, J. P. Wolfgang and M. Morteza, *Trends Biotechnol.* 2012, 30, 499-511.
81. J. A. K. Esam, E. A. O. Entisar and M. A. S. Tagreed, *Acad. J. Agric. Res.*, 2017, 6, 26-32.

- 1  
2  
3  
4  
5  
6  
7  
8  
9  
10  
11  
12  
13  
14  
15  
16  
17  
18  
19  
20  
21  
22  
23  
24  
25  
26  
27  
28  
29  
30  
31  
32  
33  
34  
35  
36  
37  
38  
39  
40  
41  
42  
43  
44  
45  
46  
47  
48  
49  
50  
51  
52  
53  
54  
55  
56  
57  
58  
59  
60
82. A. W. Bauer, W. M. M. Kirby, J. C. Sherris and M. Truck, *Am. J. Clin. Pathol.*, 1966, 45, 493-496.
83. M. M. Rahman, M. M. Alam, A. M. Asiri and M. A. Islam, *RSC Adv.*, 2017, 7, 22627–22639.
84. M. M. Rahman, M. M. Alam and A. M. Asiri, *RSC Adv.*, 2018, 8, 960–970.
85. M. M. Rahman, M. M. Alam and A. M. Asiri, *J. Ind. Eng. Chem.* 2018, 62, 392–400.
86. M. A. Subhan, P. C. Saha, M. M. Alam, A. M. Asiri, M. Al-Mamund and M. M. Rahman, *J. Environ. Chem. Eng.*, 2018, 6, 1396–1403.
87. M. M. Rahman, M. M. Alam, A. M. Asiri and M.A. Islam, *Talanta*, 2018, 176, 17–25.
88. M. M. Alam, A. M. Asiri, M. T. Uddin, M. A. Islam and M. M. Rahman, *RSC Adv.*, 2018, 8, 12562–12572.
89. M. M. Rahman, M. M. Alam, A. M. Asiri, *J. Ind. Eng. Chem.*, 2018, 65, 300–308.
90. M. M. Rahman, M. M. Alam and A. M. Asiri, *New J. Chem.* 2018, 42, 10263-10270
91. M. A. Subhan, P. C. Saha, M. M. Rahman, J. Ahmed, A. M. Asiri and M. Al-Mamun, *New J. Chem.*, 2018, 42, 872-881.
92. M. A. Subhan, P. C. Saha, M. M. Rahman, M. A. R. Akand, A. M. Asiri and M. Al-Mamun, *New J. Chem.*, 2017, 41, 7220-7231.
93. M. M. Rahman, M. M. Alam, M. M. Hussain, A. M. Asiri and M. E. M. Zayed, *Environmental Nanotechnology, Monitoring & Management*, 2018, 10, 1-9.
94. M. M. Rahman, M. M. Alam, A. M. Asiri and M.R. Awual, *New J. Chem.*, 2017, 41, 9159-9169.
95. M. M. Rahman, M. A. Hussein, K. A. Alamry, F. M. Al-Shehry and A. M. Asiri, *Nano-Structures & Nano-Objects*, 2018, 15, 63-74.
96. G. Scandurra, A. Antonella, C. Ciofi, G. Saitta and M. Lanza, *Sensors*, 2014, 14, 8926–8939.

## Table of Content (TOC):

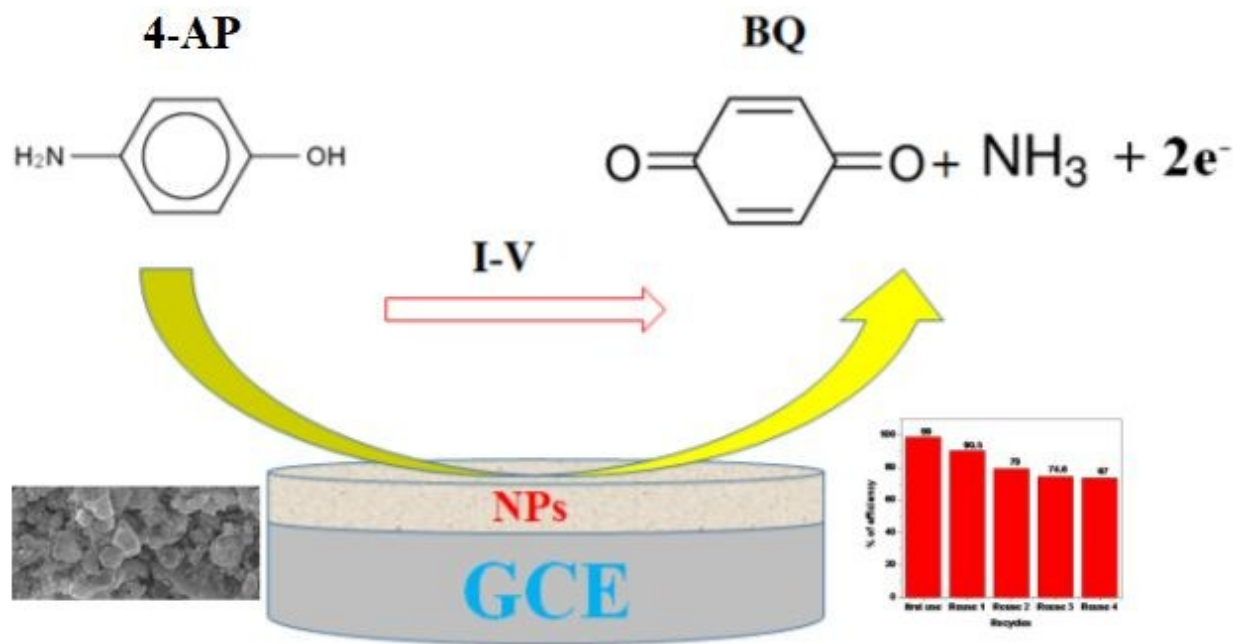


**Table of Content (TOC):**

The electrochemical oxidation of 4-AP based on  $\text{Ag}_2\text{O}_3 \cdot \text{SnO}_2 \cdot \text{Cr}_2\text{O}_3$  NPs/binder/GCE sensor.

1  
2  
3  
4  
5  
6  
7  
8  
9  
10  
11  
12  
13  
14  
15  
16  
17  
18  
19  
20  
21  
22  
23  
24  
25  
26  
27  
28  
29  
30  
31  
32  
33  
34  
35  
36  
37  
38  
39  
40  
41  
42  
43  
44  
45  
46  
47  
48  
49  
50  
51  
52  
53  
54  
55  
56  
57  
58  
59  
60